2010

Fabric development in cm-scale shear zones in ultramafic rocks, Red Hills, New Zealand

Caroline Webber
Julie Newman, *Texas A&M University*
Caleb Holyoke
Timothy Little
Basil Tikoff, *University of Wisconsin - Madison*

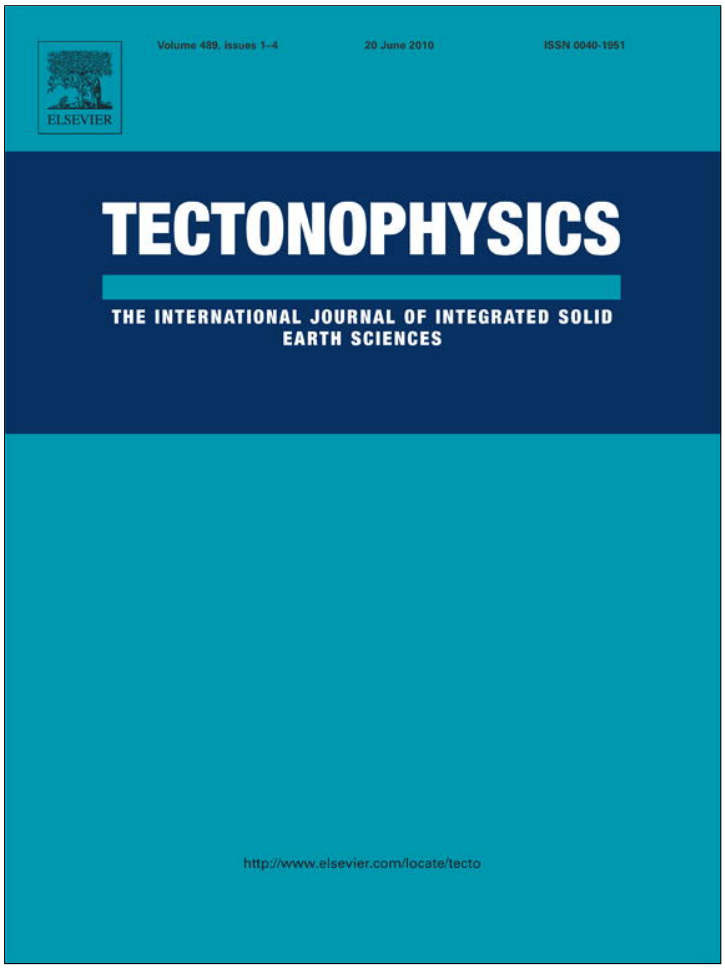

Tectonophysics 489 (2010) 55–75

Contents lists available at ScienceDirect

Tectonophysics

journal homepage: www.elsevier.com/locate/tecto

Fabric development in cm-scale shear zones in ultramafic rocks, Red Hills, New Zealand

Caroline Webber [a], Julie Newman [b,*], Caleb W. Holyoke III [b,1], Timothy Little [c,2], Basil Tikoff [a,3]

[a] University of Wisconsin, Madison, 1215 W. Dayton Street, Madison, WI 53706, United States
[b] Texas A&M University, College Station, TX 77843, United States
[c] Victoria University of Wellington, Wellington 6000, New Zealand

ARTICLE INFO

Article history:
Received 14 July 2008
Received in revised form 19 March 2010
Accepted 1 April 2010
Available online 11 April 2010

Keywords:
Upper mantle
Olivine
Lattice preferred orientation
Shear zone
Overprinting
New Zealand

ABSTRACT

The Red Hills ultramafic massif, the South Island, New Zealand, contains a suite of cm-scale shear zones that are composed of dunite, pyroxenite, and olivine websterite. Offset on these shear zones was measured using displacement of cross-cutting dikes or distinct compositional foliation layers in the host rock, and is interpreted to occur by dominantly simple shear. Shear zones contain microstructures similar to the host rock, including coarse grain sizes (>1 mm) and dominantly polygonal grains. The olivine lattice preferred orientation (LPO) in the host rocks is consistent with the (010)[100] slip system, active at high-temperature, dry upper mantle conditions. Within the shear zones, the olivine LPO, when plotted relative to the shear zone foliation and lineation, suggests (010)[001] slip. The shear zone LPO is typically more poorly clustered than in host rock samples and double maxima are observed in some samples, with the second maxima suggesting (010)[100] slip.

When olivine LPO from both host rock and shear zone samples is plotted within the same (geographic) reference frame, it is apparent that the shear zone LPO retains evidence for the dominant LPO of the host rocks. The LPO in the shear zone rocks reflects the pre-existing fabric; the poorly clustered data and double maxima reflect the changes that developed during shear zone deformation. These rocks demonstrate the influence of pre-existing LPO on textures formed during deformation and the need to consider the LPO of deformed rocks within different reference frames.

1. Introduction

Localized deformation is observed in exposures of upper mantle rocks from many settings (Dijkstra et al., 2004 and references therein). Mantle shear zones generally have a composition similar to the host rock, but with distinct microstructures and olivine lattice preferred orientation (LPO) (e.g., the Othris massif (Dijkstra et al., 2002), Voltri massif (Hoogerduijn Strating et al., 1993), the Ronda massif (van der Wal and Vissers, 1993), and the Oman ophiolite (Boudier et al., 1988; Michibayashi and Mainprice, 2004; Michibayshi et al., 2006)). A range of weakening mechanisms resulting in localization have been suggested based on both experimental and field data, including the local presence of melt (Hirth and Kohlstedt, 1995; Bai et al., 1997; Holtzman et al., 2003) or water (Mizukami et al., 2004), or a reduction in grain size causing a change in deformation mechanisms (Boullier and Gueguen, 1975; Newman et al., 1999; Dijkstra et al., 2002; Warren and Hirth, 2006) or slip systems (Jin et al., 1998).

The Red Hills ultramafic massif contains a suite of small-scale shear zones that cross-cut the previously homogeneously deformed host rock. Unlike other shear zones reported in ultramafic rocks, these shear zones are compositionally distinct from the host rock, yet contain grainsizes and microstructures similar to the host rock. When LPOs are plotted relative to the foliation and lineation in the shear zone, they suggest apparent slip along (010)[001], an atypical slip system for upper mantle rocks. However, comparison of LPOs in shear zone rocks and host rocks, viewed in the same (geographic) reference frame, indicates that the shear zone rocks contain evidence for an olivine LPO that is the same as the host rock LPO, as well as evidence for later deformation by slip along (010)[100], a more commonly recognized slip system in naturally deformed mantle rocks, suggesting that the host rock LPO was present in the shear zone rocks prior to shearing. The pre-existing LPO of the homogeneously deformed host rock influenced the resulting LPO preserved in shear zone rocks after localized deformation.

* Corresponding author. Fax: +1 979 845 6162.
E-mail addresses: cwebber@geology.wisc.edu (C. Webber), newman@geo.tamu.edu (J. Newman), holyoke@geo.tamu.edu (C.W. Holyoke), timothy.little@vuw.ac.nz (T. Little), basil@geology.wisc.edu (B. Tikoff).
[1] Fax: +1 979 845 6162.
[2] Fax: +64 4 463 5186.
[3] Fax: +1 608 262 0693.

0040-1951/$ – see front matter © 2010 Elsevier B.V. All rights reserved.
doi:10.1016/j.tecto.2010.04.001

This study of LPOs in naturally deformed mantle shear zones and their host rocks demonstrates: 1) the influence of a pre-existing LPO on the evolution of LPO during deformation along localized zones; 2) the necessity of comparing host rock LPOs with LPO in shear zone rocks; and 3) the advantages of plotting LPOs in multiple reference frames.

2. Geologic setting of Red Hills study area

2.1. Regional geology of the Red Hills study area

The Red Hills massif (~100 km^2) is located in the northern portion of the South Island, New Zealand (Fig. 1). It is part of the Dun Mountain Ophiolite Belt (DMOB), a package of mafic–ultramafic rocks and structurally overlying sediments that is discontinuously exposed for >1100 km (Fig. 1B). The DMOB is divided into two segments dextrally offset by ~460 km on the Alpine Fault. The DMOB is up to ~8 km wide (Davis et al., 1980) and gravity surveys indicate that the northern, Red Hills part of the ultramafic body is <4 km thick (Malahoff, 1965). The Red Hills massif is mostly unserpentinized and provides significant horizontal exposure (~100 km^2) and vertical relief (>700 m).

2.2. Previous work in the Red Hills area

Walcott (1965) conducted the first structural study of the Red Hills massif and mapped (1:50,000) a ~260 km^2 region that includes the Red Hills and adjacent areas. At Porter's Knob (Fig. 2), Walcott (1965) identified two foliations: 1) A north-dipping compositional foliation defined by banded dunite and harzburgite; and 2) a cross-cutting south-dipping "metamorphic foliation." The cross-cutting "foliation" was defined by dunite layers that he interpreted to have formed as replacement features, and by pyroxenite zones that he interpreted to have been injected as melt after the dunite layers formed. Walcott (1965) described shear deformation in the south-dipping dunite bands and suggested that deformation occurred simultaneously with metasomatic formation of the dunite.

Both Walcott (1965) and Christensen (1984) measured olivine LPO in samples from the Red Hills. Walcott (1965) described a similarity of LPO in host rock and the cross-cutting, south-dipping zones. Christensen (1984) measured LPOs in olivine from the western side of the Red Hills field area and determined that the LPOs measured in Red Hills are similar to those measured in other ultramafic massifs and are consistent with deformation dominantly by dislocation creep with glide on the (010)[100] slip system.

Webber (2005) and Webber et al. (2008) mapped a ~2 km^2 region of the Red Hills near Porter's Knob and identified four structural domains defined by superposed fabrics (Fig. 2), with the Central Domain fabrics, the focus of this study, the oldest recognized in the area. The Central Domain contains north-dipping banded harzburgites and dunites, and is overprinted by a 50 m thick domain of south-dipping shear as well as cm-scale south-dipping shear zones.

2.3. Porter's Knob lithology and structure

2.3.1. Host rock

The Porter's Knob area is composed dominantly of harzburgite (~90%) with local lherzolite and dunite. Compositional foliation is north-dipping, defined by the alternation of 2–3 cm thick layers of olivine-rich (>90% olivine) or olivine-poor (<90% olivine) composition (Fig. 3), and is deformed into open folds with amplitudes of <10 cm. Elongate spinel and orthopyroxene grains and oriented aggregates of spinel define a lineation in compositional layers. The mean orientation of foliation is 277 50°N, in which the lineation plunges shallowly to the E or W. The rocks that exhibit this N-dipping

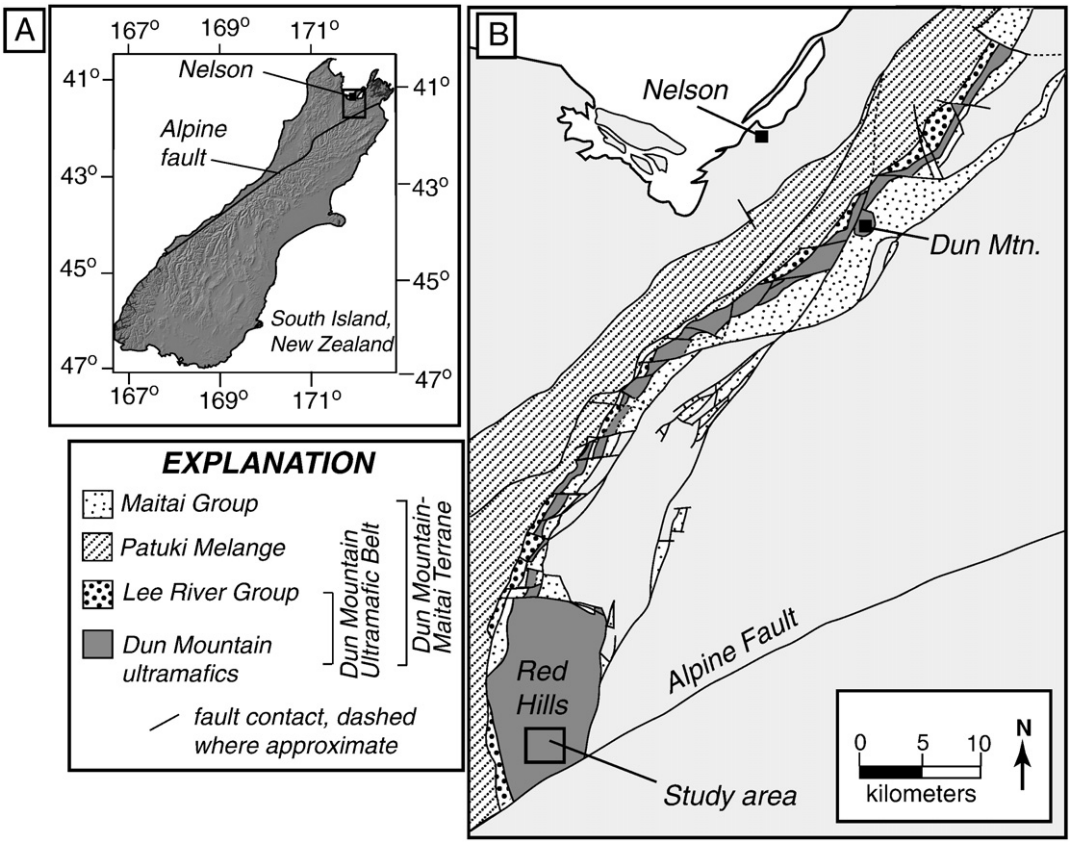

Fig. 1. Location of Red Hills study area. (A) Digital elevation model of South Island, New Zealand illustrating location of Alpine Fault (data from www.geographix.co.nz). Box denotes area of image in part B. (B) Map of the northern segment of the Dun Mountain Ophiolite Belt. Note location of Red Hills ultramafic massif and the study area.

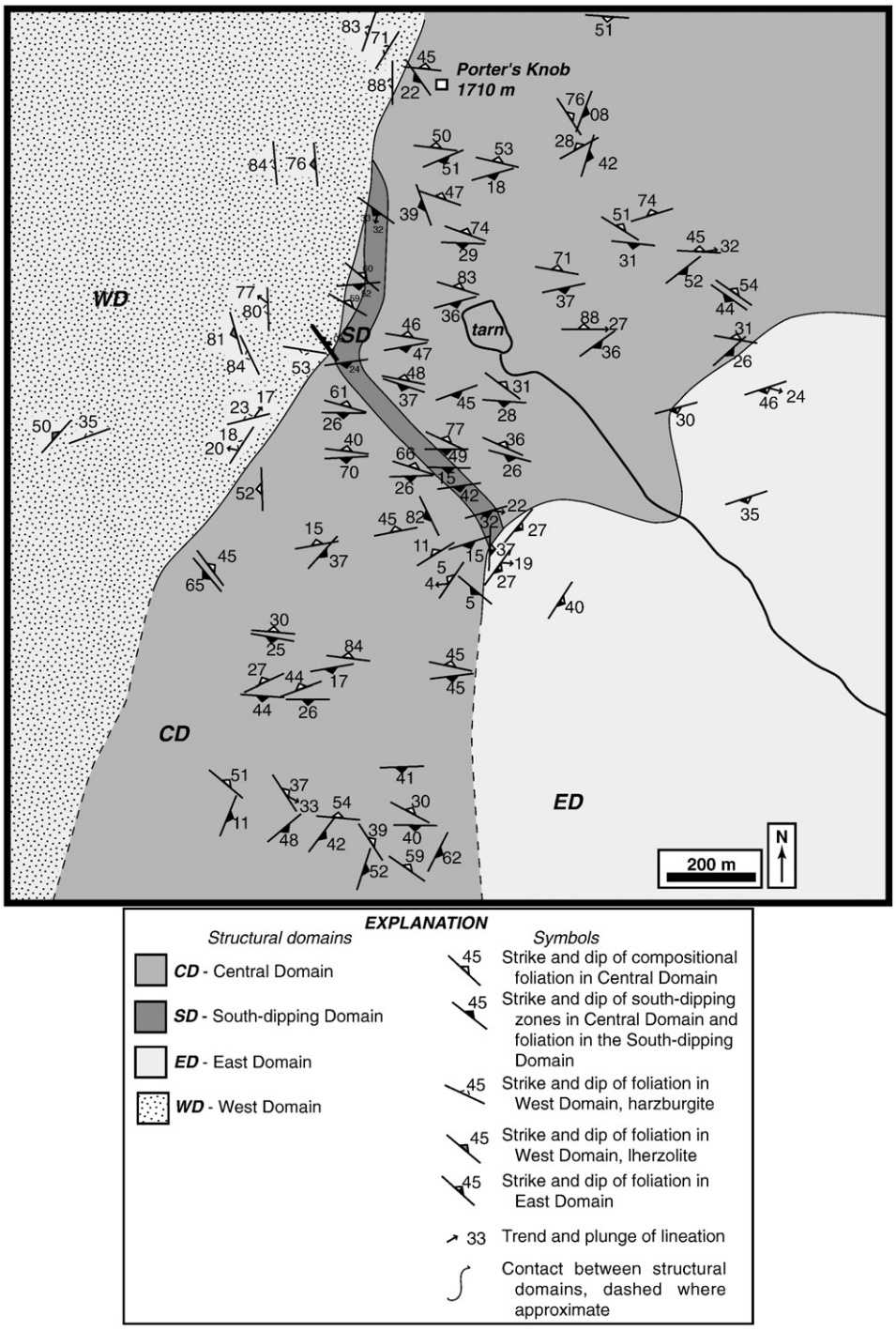

Fig. 2. Structural domain map of the Red Hills study area (after Webber et al., 2008).

compositional foliation are referred to as host rocks throughout the remainder of this paper.

The dominant microstructures observed in the host rocks (Fig. 4A) are 120° triple junctions in olivine and a well-defined grain-shape preferred orientation in olivine and pyroxene that is parallel to the spinel elongation direction. Grain size is coarse in all lithologies, typically 1–5 mm in harzburgite and ≤10 mm in dunite. Host rocks are characterized by a bimodal distribution of olivine grains (coarse grains: 2–5 mm; fine grains: 1–3 mm) (porphyroclastic peridotite texture; Mercier and Nicolas, 1975).

Olivine grain boundaries are straight to slightly curvilinear, and grain shapes are moderately flattened (~7:4) parallel to lineation and perpendicular to foliation. Subgrains and smaller, recrystallized grains are also observed. Orthopyroxene grains are irregularly shaped or slightly elongate and range up to ~3 mm in diameter, but most are 1–2 mm. Commonly, orthopyroxene contains ≤5 μm wide clinopyroxene exsolution lamellae and some samples contain spinel exsolution (≤1 μm wide). Orthopyroxene typically has a poikiloblastic texture, containing abundant inclusions of olivine (≤1 mm). Clinopyroxene is irregularly shaped and is 0.5–1 mm in diameter. Spinel occurs as inclusions in olivine grains or concentrated on olivine grain boundaries. Spinel grains that are 0.2–0.5 mm long define an elongation lineation, and planes containing abundant spinel are subparallel to the compositional layering. Plagioclase occurs in some

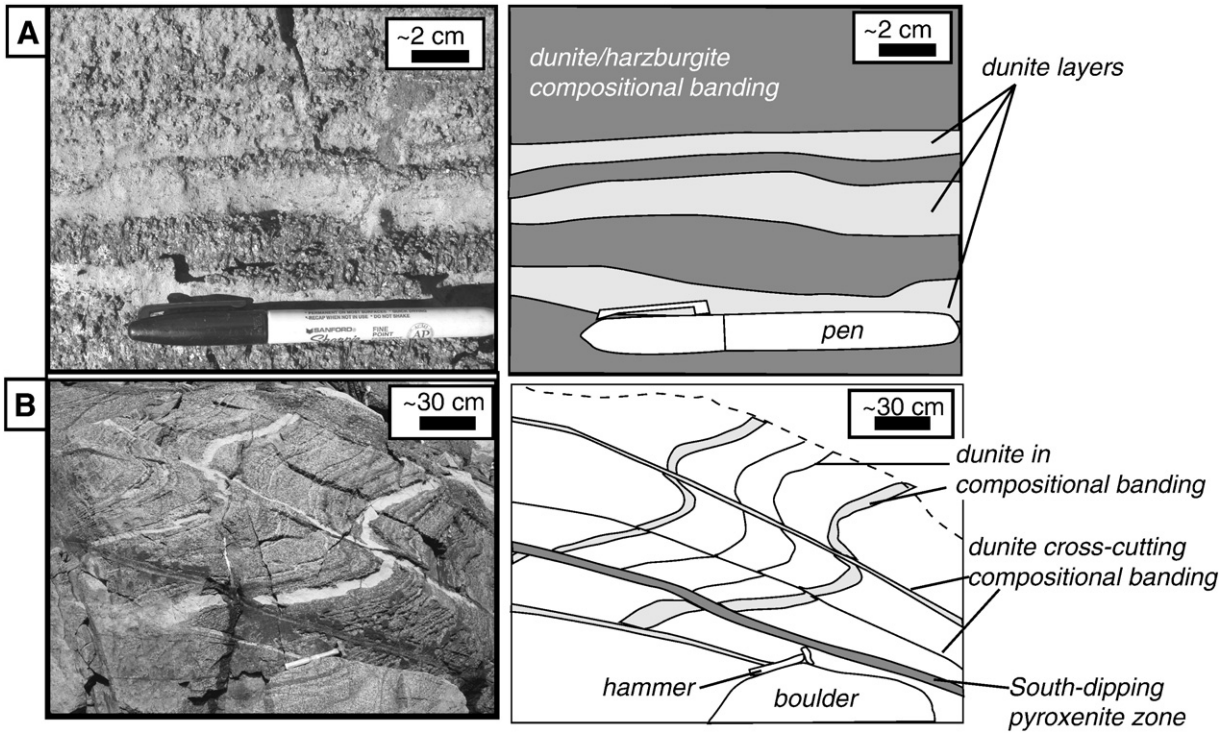

Fig. 3. Compositional banding in the host rock. (A) Image and sketch of compositional banding defined by alternating dunite and harzburgite layers at the hand sample scale. (B) Image and sketch of outcrop located at Porter's Knob, illustrating compositional banding and cross-cutting, south-dipping, dunite and pyroxenite zones.

harzburgite and lherzolite outcrops as elongate (5:3) grains that are ~1 mm long with curved grain boundaries. Plagioclase, where present, forms bands that are <5 mm wide and parallel compositional foliation or small-scale shear zones.

2.3.2. Discordant tabular zones

Tabular zones of dunite, pyroxenite and olivine–websterite cross-cut the host rock compositional foliation (Fig. 3). Dunite bodies are primarily south dipping (Fig. 5A), have sharp contacts with the host rock layering, and range in thickness from 2 to 50 cm. Thin zones of clinopyroxene occasionally, and only locally, mark the contact between the dunite and the host rock. Pyroxenite tabular zones occur in a wide range of orientations (Fig. 5B) and are occasionally folded or exhibit boudinage. Contacts between pyroxenite zones and host rocks are typically poorly defined. Pyroxenite zones are generally 1–10 cm thick, but one distinctive population of clinopyroxenite zones is <1 cm thick. Cross-cutting relationships indicate several generations of cross-cutting tabular zones are present.

Approximately 20% of the observed cross-cutting tabular zones (dunites and pyroxenites) exhibit measurable offset of distinctive features (e.g., distinctive compositional bands) across them. These zones are interpreted to be shear zones. The majority of the shear zones are south-dipping, but 4 shear zones occur in north-dipping orientations (all pyroxenites). Shear zones range in thickness from <1 cm to ~50 cm (3–10 cm is most common). The amount of offset varies from 2 to 90 cm, measured from displaced dikes or distinct compositional bands. Interestingly, both normal and reverse shear sense is observed.

Foliation and lineation in shear zones is difficult to determine in outcrop because the shear zone plane is almost never exposed in three dimensions. In hand sample and thin section, foliation is defined by linear aggregates of spinel grains that strike ESE and dip moderately SSW. Lineation is subparallel to the dip direction (S) in outcrop, though it is rarely observed.

Microstructures in shear zones are similar to those in the host rocks (Fig. 4B). Well-developed 120° triple junctions and mostly planar boundaries are common in olivine grains. In some examples, olivine grains are flattened and show a well-developed grain-shape preferred orientation that is parallel to host rock compositional banding. Grain size is similar to host rocks, with the olivine mean grain size ~2–5 mm.

2.4. Estimate of deformation conditions at Porter's Knob

Deformation temperatures, based on two-pyroxene geothermometry (Brey and Köhler, 1990; Taylor, 1998), suggest 875–1025 °C in north-dipping compositional layering, and 750–850 °C in the shear zones, though one shear zone sample yields 925–950 °C (Webber, 2005; Webber et al., 2008). These temperature estimates may reflect minimum temperatures due to possible re-equilibration following deformation. Webber (2005) reports pressure estimates of ~1 GPa.

3. Field and laboratory methods

3.1. Strain measurements

Apparent offset of distinctive layers across the cm-scale shear zones was measured in the field. Displacement magnitude was estimated from field measurements by constructing sections parallel to the fault plane and projecting the trace of the offset marker onto the slip plane (e.g., Marshak and Mitra, 1988). Because of the difficulty in recognizing lineation in the shear zone rocks, it is assumed in slip measurements that the transport direction is the same for all shear zones and is parallel to the mean lineation azimuth of 179°. This mean lineation azimuth is also used as the reference measurement for orientation of olivine LPO data.

Shear and finite strain calculations were made assuming only simple shear. Shear strain (γ) was calculated by dividing displacement by the thickness of the zone. The finite strain ratio (R) was calculated using the equations of Tikoff and Fossen (1993).

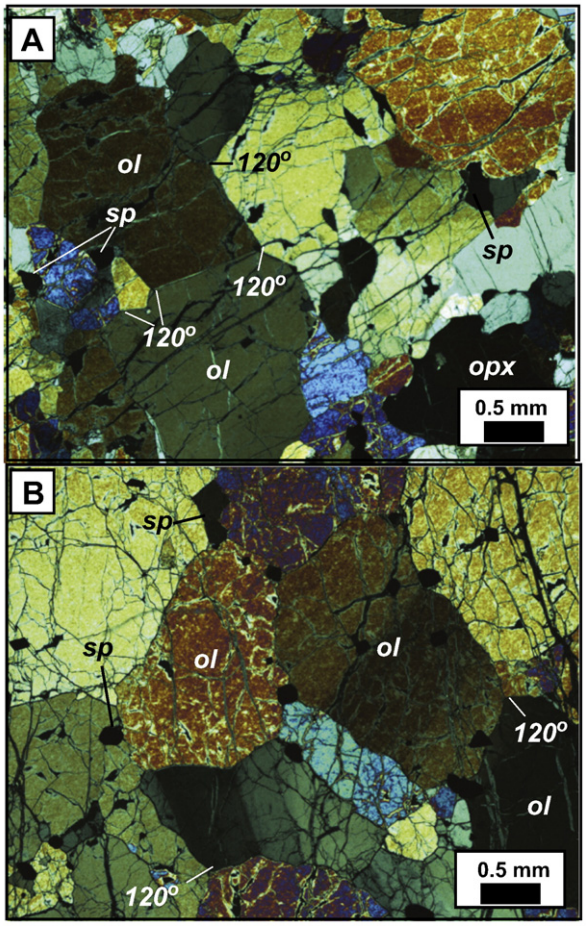

Fig. 4. Photomicrographs illustrating microstructures of host rock and cross-cutting shear zones. Both views are of thin sections oriented parallel to lineation and perpendicular to foliation. ol — olivine, opx — orthopyroxene, sp — spinel. (A) Sample from host rock (harzburgite). Note 120° triple junctions and several smaller (recrystallized) grains. (B) South-dipping dunite zone. Grain size and microstructures are similar to those features in the host rock, including 120° triple junctions, recrystallized grains and sharp extinction. Crossed polars.

3.2. Olivine LPO data

Olivine LPOs are reported here for samples collected from four representative shear zones and surrounding host rock (Fig. 6). LPOs and descriptions of other shear zones from the Red Hills are reported in Webber (2005). The orientations of [100], [010] and [001] of at least 95 olivine grains from each sample were measured using a 5-axis universal stage and plotted on a lower-hemisphere equal area net using the Kamb (1959) method with a contour interval of 2 sigma.

We have plotted the olivine LPO data for each sample in two different reference frames. First, for all sample localities, we present the data in a sample specific reference frame, with shear zone samples plotted relative to shear zone foliation and lineation (determined as described above) and host rock samples plotted relative to host rock foliation and lineation (Figs. 7–10). Second, for shear zones RH04-9 (Fig. 7), RH04-12 (Fig. 8), and RH04-22 (Fig. 9) we have also presented the data in a geographic reference frame, i.e. presenting the LPO data rotated with respect to geographic coordinates so that north on the stereonet represents geographic north. This presentation method is useful for identifying similarities in orientation of olivine LPO in different structures (e.g., host rock and shear zones). For shear zone RH04-15, in an out-of-place boulder, we have plotted the LPO data for each sample relative to 1) the shear zone foliation and lineation, and 2) relative to the host rock foliation and lineation (Fig. 10), as we cannot know the geographic reference frame.

4. Results: olivine LPO data

Below we report data for the host rock olivine LPO in the Central Domain and for 4 representative shear zones and their adjacent host rock (Fig. 6). For each shear zone sample site, we present a description of structures in the outcrop, estimates of shear and finite strain, and the olivine LPO data. The thicknesses of the zones and the calculated finite strain are given in Table 1.

4.1. Host rock LPO

Viewed in the geographic reference frame, host rock olivine [100] form a point maximum plunging shallowly to the E–SE, [010] generally plunge steeply W–NW, and [001] plunge shallowly in a NE or SW direction (Figs. 7 and 8), although [010] and [001] form diffuse to partial girdles in some samples. When plotted in the sample reference frame (foliation: 277 50° N; lineation plunges shallowly to the E or W), [100] are parallel, or at a low angle, to lineation within the foliation, and [010] and [001] form (partial) girdles perpendicular to foliation (e.g., Figs. 8, sample 12D and 10, sample 15I.) In some samples, [001] form diffuse maxima at a low angle to lineation (e.g., Fig. 7, samples 9F and RH2). Minor variations in the LPO of the host rock are observed in host rock samples obtained from locations near shear zones; the details are discussed below for each outcrop.

4.2. Outcrop RH04-09: offset on two south-dipping dunite shear zones

Outcrop RH04-09 contains two dunite shear zones (<10 cm thick) that dip south and offset the older compositional foliation in the host rock (Fig. 7). The host rock is composed of harzburgite, and contains two distinctive bands of dunite that are oriented parallel to the compositional layering. These dunite bands are crosscut and offset by the two shear zones (zones A and B). Offset along zone A is 114 cm ($\gamma = 11$; $R = 132$) and offset along zone B is 10 cm ($\gamma = 5$; $R = 27$).

Sample 9F, from ~40 cm above shear zone A, should most closely represent the Central Domain LPO. The other host rock samples are located between the two shear zones and may have been affected by strain associated with the shear zone deformation. Sample 9F, viewed in the sample reference frame with respect to the host rock foliation and lineation, contains [100] at a low angle to the lineation, [010] form a girdle perpendicular to the foliation and lineation. [001] contain a weak girdle subperpendicular to the foliation and lineation (Fig. 7C). The samples are also plotted within a geographic reference frame. Viewed in the geographic reference frame, the other host rock samples and the shear zone samples display LPOs similar to 9F, with some modification. Shear zone [100] are rotated clockwise (towards N), with respect to the host rock samples, and [001] are more diffuse than in host rock samples.

When the shear zone samples are plotted in the sample reference frame relative to the shear zone foliation and lineation, [100] form a point maximum perpendicular to the transport direction in the plane of the shear zone. [010] are perpendicular to the shear plane in the plane containing the lineation, and [001] are diffuse, although a weak maximum of [001] parallel to the transport direction is observed in 9D and RH3.

Data from shear zone A (9E and 9D) and shear zone B (9A and RH3) do show some differences, however. In shear zone B, [100] are more diffuse than in shear zone A, and form a girdle parallel to the plane of the shear zone. [010] form a point maximum subperpendicular to the plane of the shear zone.

Comparison of dunite (9F, RH1 and RH2) and harzburgite (9C and 9B) host rock samples also yields some differences. While the orientations of axes are similar, harzburgite olivine LPO are more diffuse and are rotated with respect to the dunite host rock olivine LPO. [001] in harzburgite samples are particularly diffuse relative to the dunite [001].

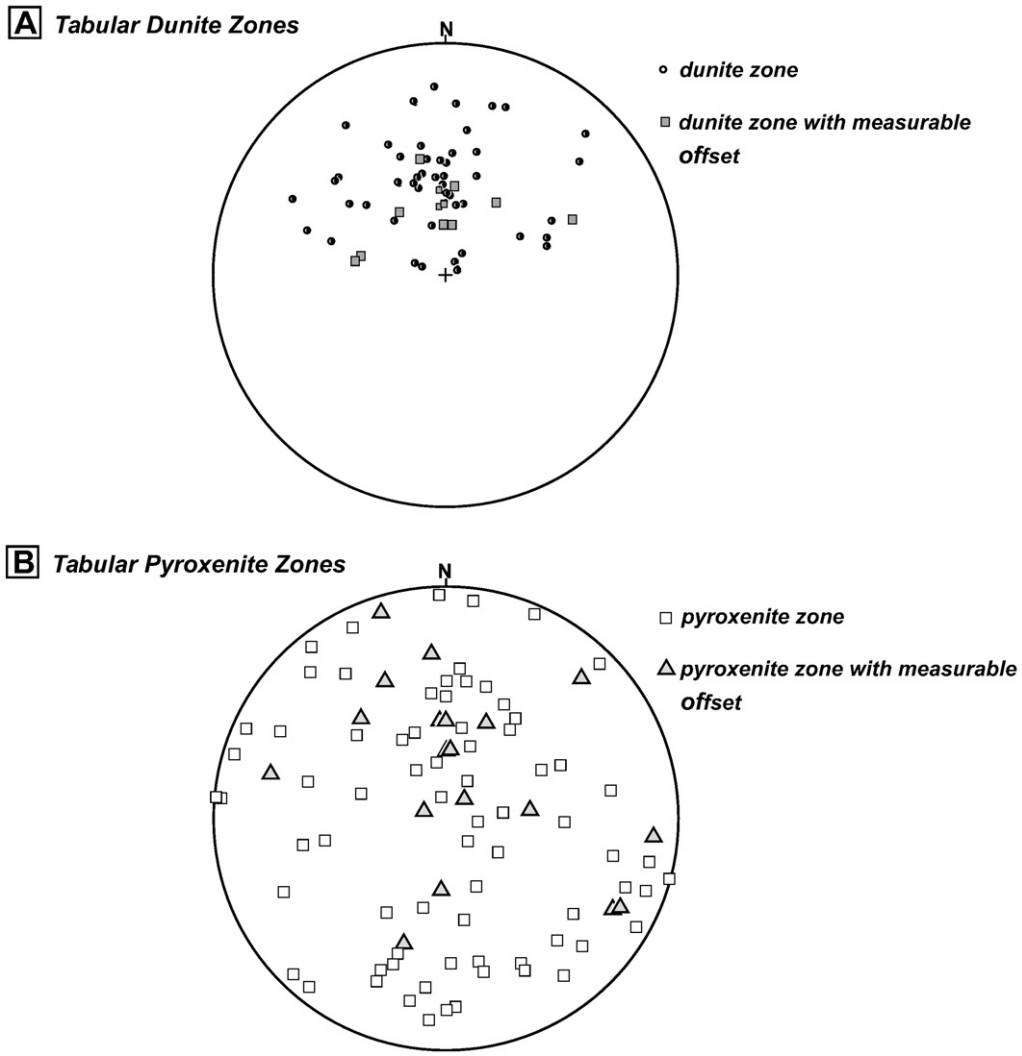

Fig. 5. (A) Orientation of tabular dunite zones and a population of those zones that contain visible offset. (B) Orientation of tabular pyroxenite zones and a population of those zones that contain visible offset. Lower hemisphere equal area nets. Poles to planes.

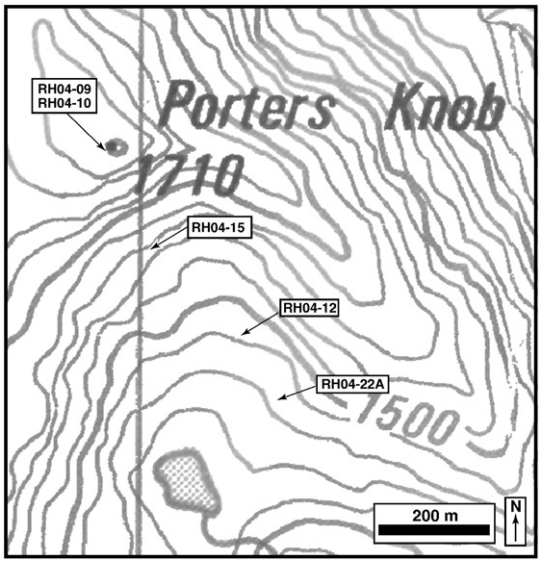

Fig. 6. Topographic map of a portion of the Red Hills field area with sample locations.

In summary, in the geographic reference frame, shear zone and host rock samples have similar LPOs. Data from samples from shear zone A, presented in the sample reference frame of the shear zone foliation and lineation, contain a maximum of [100] perpendicular to the lineation in the plane of the shear zone; data from samples from shear zone B display a girdle of [100] parallel to the plane of the shear zone. In the sample reference frame, shear zone [100] are rotated clockwise with respect to the host rock maximum, [001] form weaker maxima in shear zone samples than in host rock samples, and olivine LPO in harzburgite host rock samples are weaker than in dunite host rock samples.

4.3. Outcrop RH04-12: offset and boudinage of an orthopyroxenite dike in a dunite shear zone

Outcrop RH04-12 contains a 10 cm thick dunite shear zone that offsets a 3 cm thick folded orthopyroxenite dike (Fig. 8). The host rock at RH04-12 is a harzburgite. The orthopyroxenite dike is displaced 47 cm (reverse displacement) by the south-dipping dunite shear zone ($\gamma = 5.5$; $R = 32$) and exhibits boudinage within the shear zone (Fig. 8A and B).

Olivine LPO was determined in two samples from the shear zone and in one sample from the harzburgite host rock (Fig. 8C). Viewed in the geographic reference frame, all samples have a similar LPO, although patterns in the shear zone samples are more diffuse and form double maxima.

In the host rock sample reference frame, the harzburgite host rock sample contains [100] parallel to the lineation. [010] and [001] form girdles perpendicular to the lineation. In shear zone sample 12A viewed in the sample reference frame relative to the shear zone foliation and lineation, olivine [100] form a strong maximum ~30° from the lineation with a weaker maximum perpendicular to the lineation in the plane of the shear zone. In 12B (adjacent to an orthopyroxenite boudin), [100] form a stronger maximum perpendicular to the lineation in the plane of the shear zone with a diffuse girdle perpendicular to the plane of the shear zone and in the plane that contains the lineation. [010] in both 12A and 12B are perpendicular to the plane of the shear zone in the plane that contains the lineation. [001] in 12B form double maxima, one parallel to the lineation, and one perpendicular to the lineation in the plane of the shear zone.

In summary, in the geographic reference frame, shear zone samples contain double maxima, with one maximum close to the host rock maximum. In sample 12B, [100] that are similar in orientation to the host rock maximum are perpendicular to the lineation in the plane of the shear zone, while a second maximum is parallel to the shear zone lineation.

4.4. Outcrop RH04-22A: offset and boudinage of an orthopyroxenite dike in a dunite zone

Outcrop RH04-22A contains a south-dipping dunite shear zone that offsets a north-dipping orthopyroxenite dike (Fig. 9). The host rock at outcrop RH04-22A is banded harzburgite. The orthopyroxenite dike is boudinaged in the dunite zone and offset 5.2 cm ($\gamma = 2$; $R = 6$). The orthopyroxenite boudins unambiguously indicate a normal sense of offset (Fig. 9A and B). Host rock sampling in this exposure was unsuccessful.

Olivine LPO was measured in two samples (22A1 and 22A2) from the dunite shear zone (Fig. 9D). Sample 22A1 was collected adjacent to an orthopyroxenite boudin. When the olivine orientation data are viewed in a geographic reference frame, olivine LPO from these samples have similar orientations to samples from other exposures in the field area (e.g., sample RH04-9, Fig. 7). In the sample reference frame, sample 22A1 contains double maxima of [100], with the stronger maximum perpendicular to the shear zone lineation in the plane of the shear zone; the weaker maximum is parallel to the lineation (compare to sample 12A). [010] are oriented perpendicular to the shear plane, and [001] are oriented parallel to the lineation in the plane of the shear zone. The olivine orientation data in sample 22A2 contains a single maximum of [100] perpendicular to the lineation in the plane of the shear zone. [010] and [001] are rotated ~45° clockwise from the orientations of olivine grains in sample 22A1.

In summary, in a geographic reference frame, the olivine orientations in these samples are similar to those in other shear zone samples. In the sample reference frame, sample 22A1 contains double maxima of [100], with one approximately parallel to the shear zone lineation.

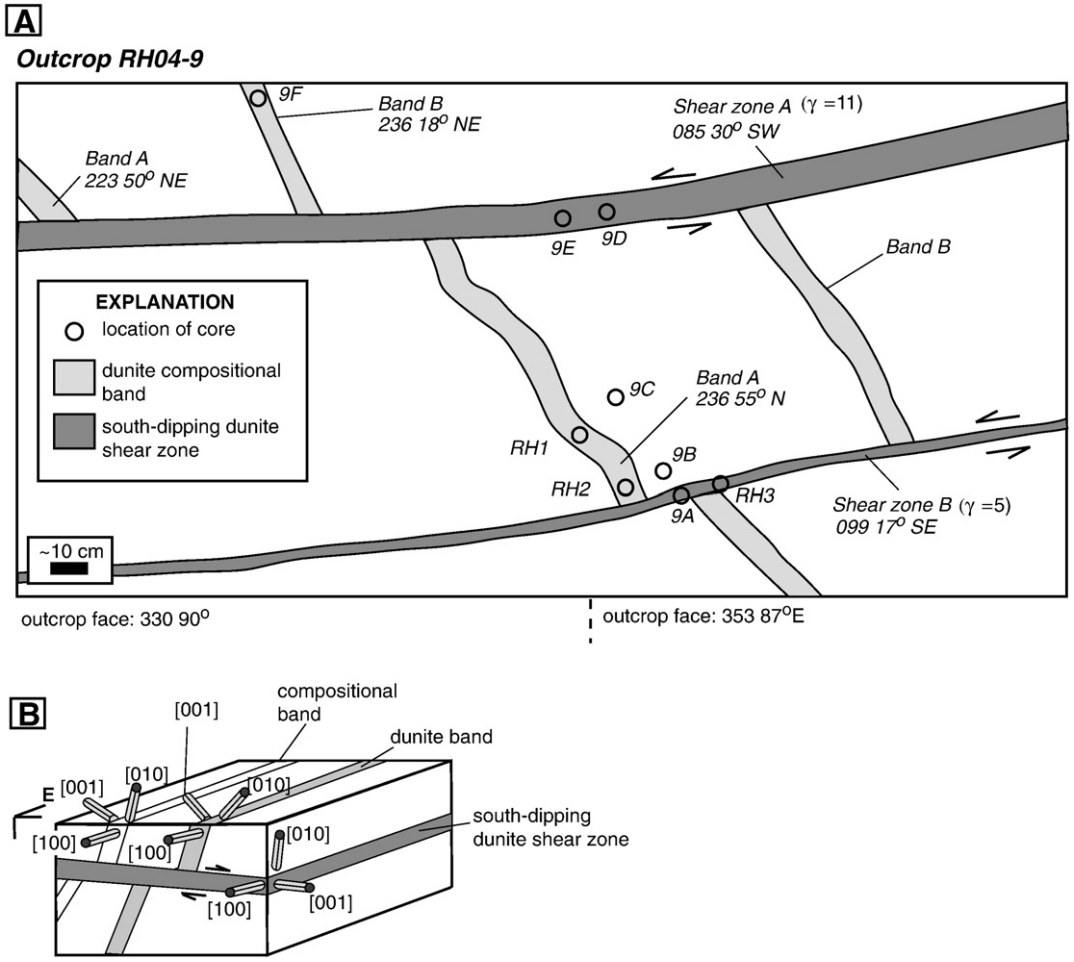

Fig. 7. Outcrop RH04-9. (A) Sketch of outcrop indicating the orientation of major structural features. (B) Block diagram illustrating the orientation of olivine axes in host rock and cross-cutting zones. (C) Olivine LPO data from four samples of shear zones and five samples of host rock in outcrop RH04-9. Data are shown in both the sample reference frame (relative to sample foliation and lineation) and the geographic reference frame (N at top of stereonets). The contour interval on all equal area nets is 2.

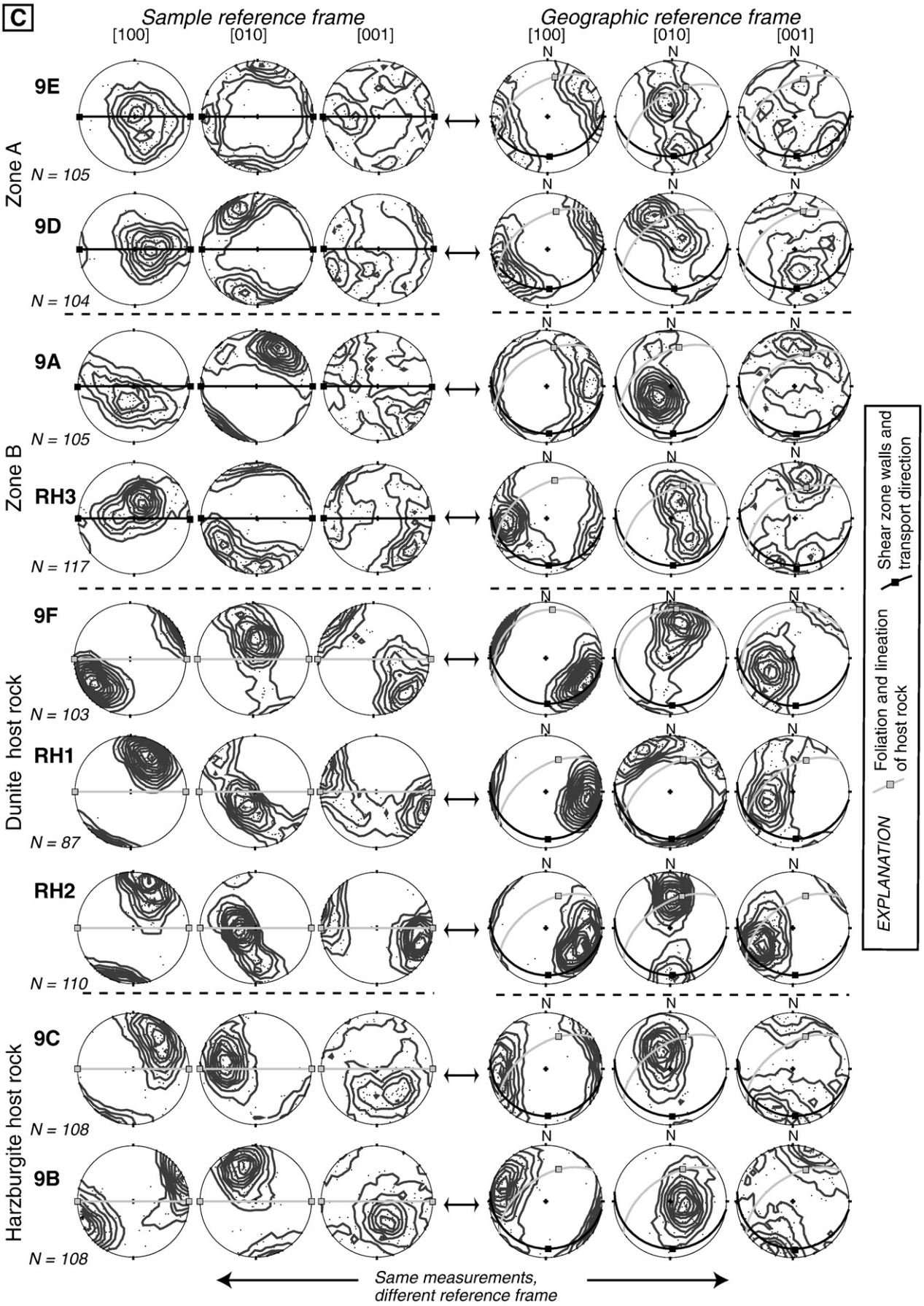

Fig. 7 (*continued*).

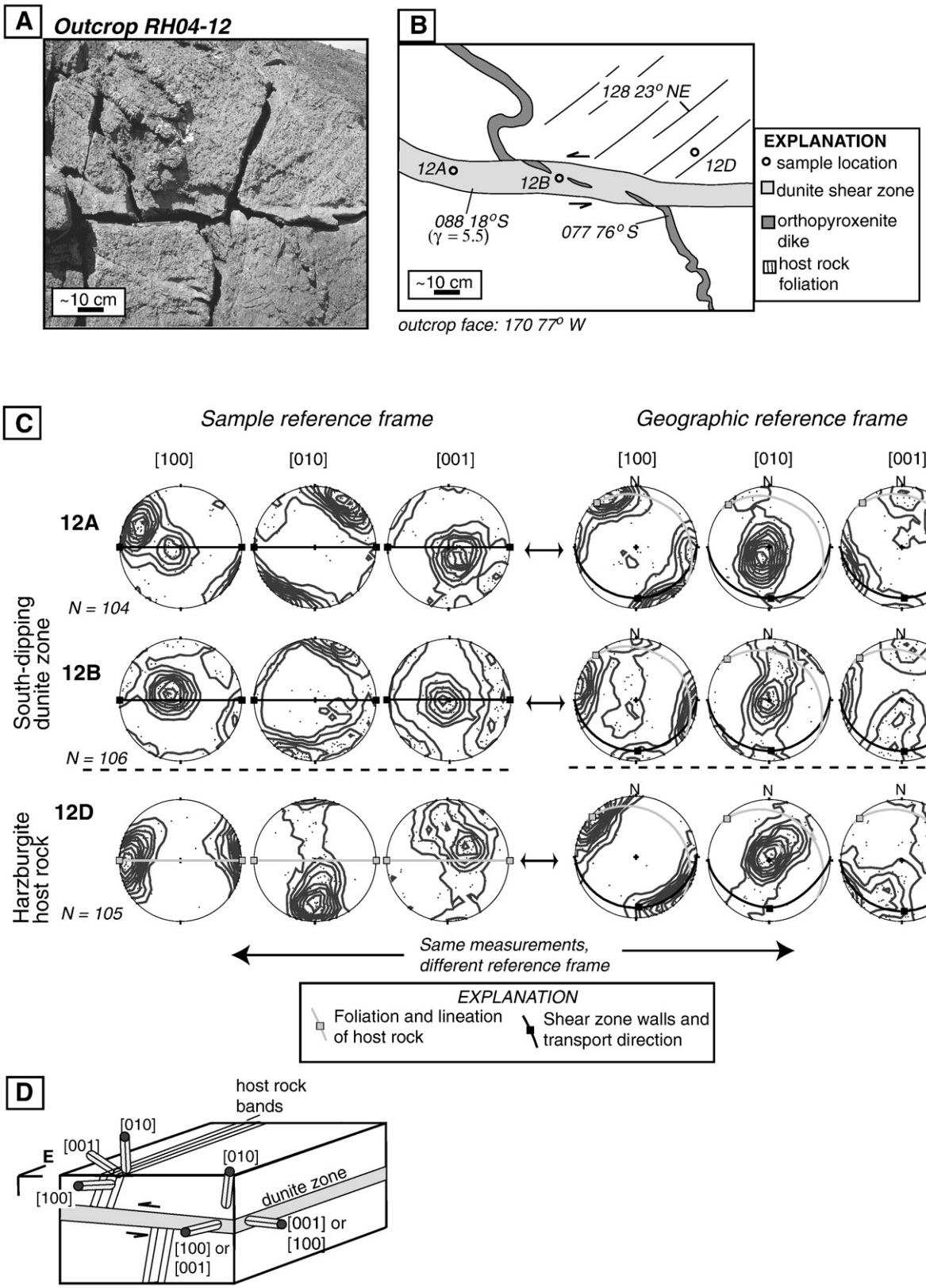

Fig. 8. Outcrop RH04-12. (A) Photo of outcrop RH04-12. (B) Sketch of outcrop indicating the orientation of major structural features. (C) Olivine LPO data from two samples in the shear zone and one sample from the host rock. Data are shown in both the sample reference frame (relative to sample foliation and lineation) and the geographic reference frame (N at top of stereonets). The contour interval on all equal area nets is 2. (D) Block diagram illustrating the orientation of olivine axes in the host rock and cross-cutting zone.

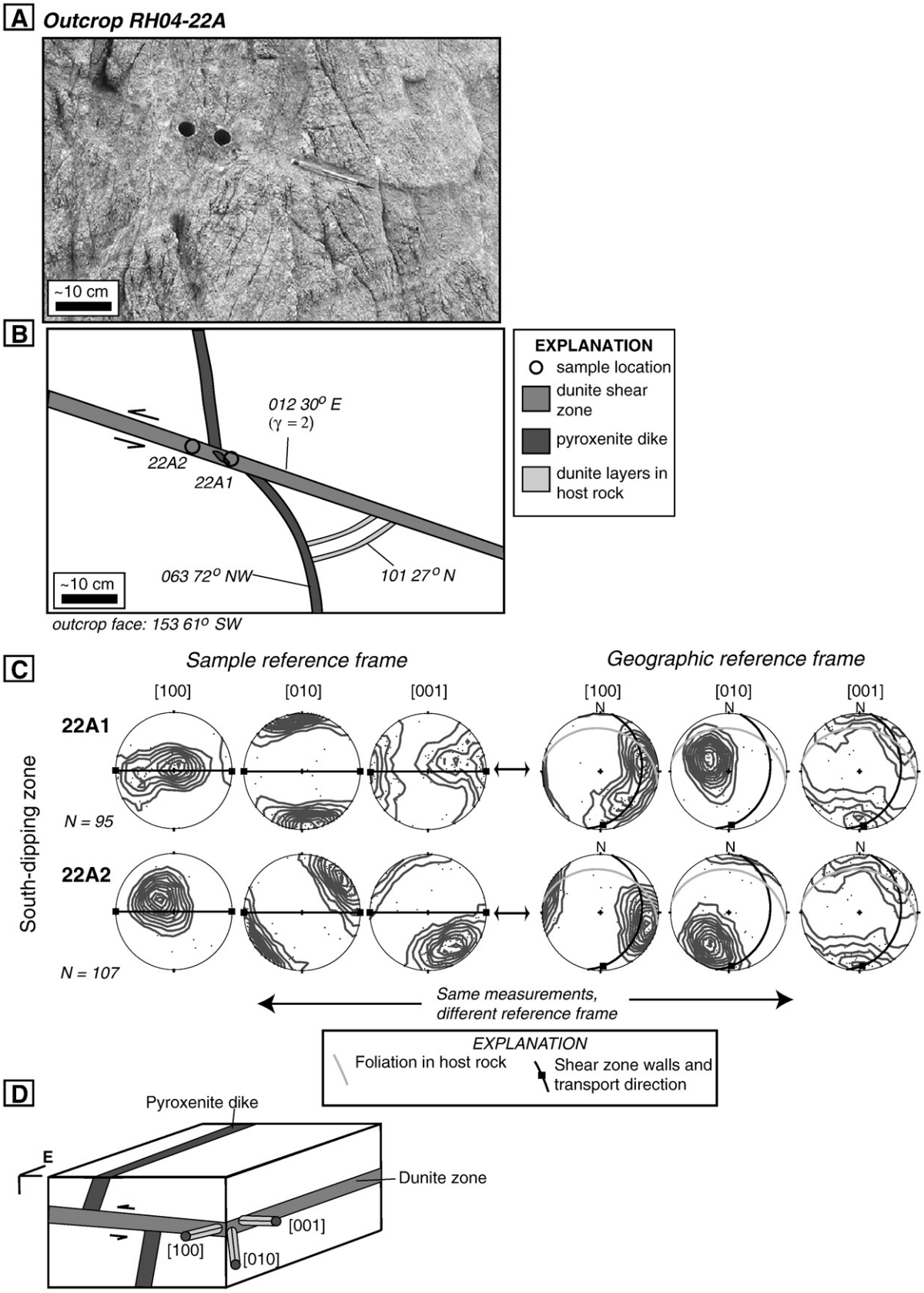

Fig. 9. Outcrop RH04-22A. (A) Photo of outcrop RH04-22A. (B) Sketch of outcrop indicating the orientation of major structural features. (C) Olivine LPO data from two samples in the shear zone in outcrop RH04-22A. Data are shown in both the sample reference frame (relative to sample foliation and lineation) and the geographic reference frame (N at top of stereonets). The contour interval on all equal area nets is 2. (D) Block diagram illustrating the orientation of olivine axes in the cross-cutting zone.

4.5. Outcrop RH04-15: rotation/drag folding of a dunite band by a crosscutting shear zone along an olivine–websterite zone

For outcrop RH04-15, an out of place boulder, we have not plotted the data in a geographic reference frame. We present the data for each sample in the sample reference frame relative to the shear zone foliation and lineation, as we have for the other outcrops, and then we also plot the data in the reference frame of the host rock foliation and lineation (Fig. 10).

Outcrop RH04-15 contains an olivine websterite zone across which two distinctive dunite layers and an olivine websterite dike are offset. The outcrop provides excellent three-dimensional exposure of the cross-cutting relationships between the offset dunite bands and offset olivine websterite dike (Fig. 10A and B). The dunite bands and olivine websterite dike are cut and offset along an olivine websterite zone (zone A; $\gamma = 4$; $R = 14$) and are rotated into, and offset along, another olivine websterite zone (zone B; $\gamma = 52$; $R = 2706$).

Outcrop RH04-15 provides an opportunity to characterize fabric within a strain gradient. In this outcrop, a distinct dunite band in the host rock is rotated into parallelism with a cross-cutting shear zone (zone B), associated with the olivine–websterite dike. Measurements of α, the angle between the shear zone and the marker layer, were obtained at five locations at distances of ≤ 25 cm from the cross-cutting shear zone. Values of γ were calculated from the measured values of α. Shear strains that range from 0.3 to 3.3 are correlated with finite strains that range from 1.4 to 12.9 (Table 2).

The orientations of olivine grains in seven samples from the host rock dunite band were measured (Fig. 10D). Two samples (15H and 15J) were collected from the dunite band where it is immediately adjacent to the olivine–websterite zone. Olivine in sample 15I (farthest from the shear zone; $\gamma = 0$), has the same LPO as olivine in the Central Domain; [100] form a maximum at a low angle (16°) to the host rock foliation and lineation (and a high angle, 55°, to the shear zone foliation and lineation), [010] form a diffuse girdle with a

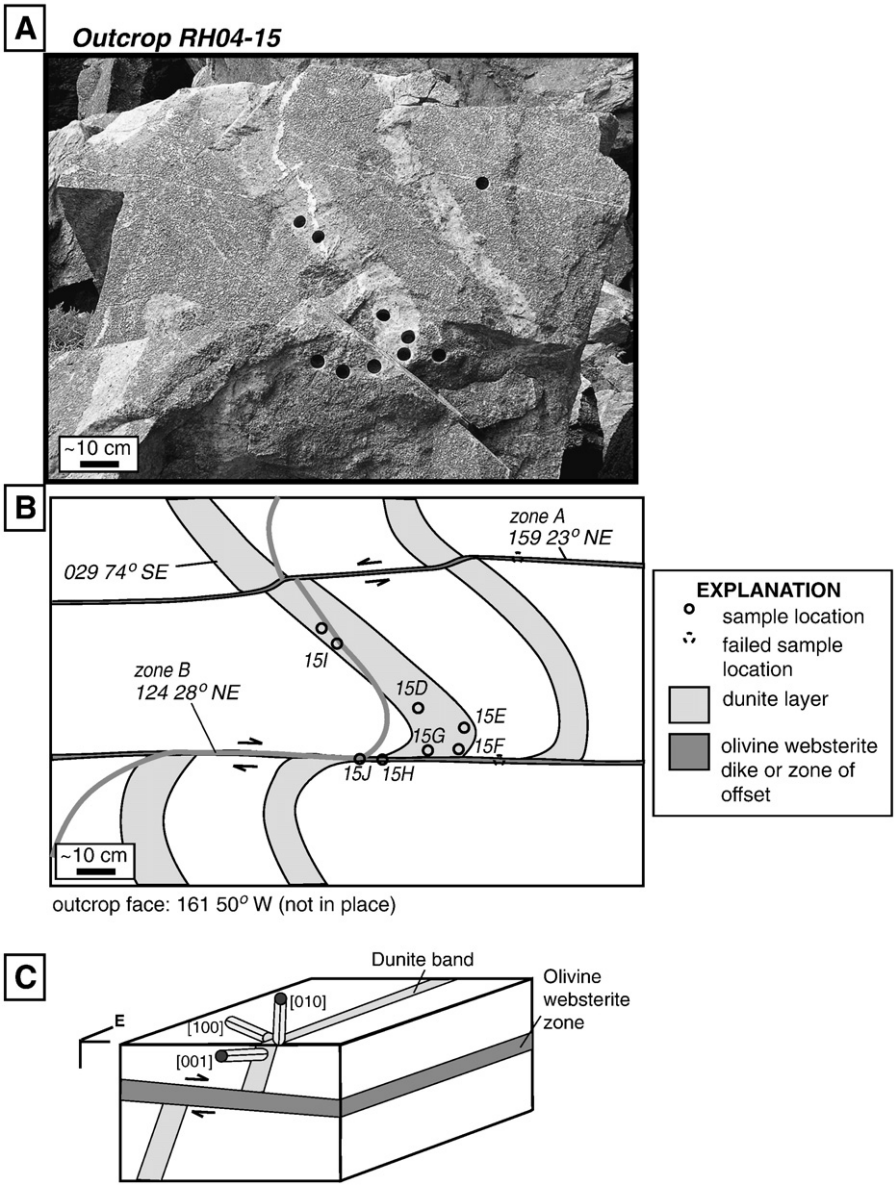

Fig. 10. Outcrop RH04-15. (A) Photo of outcrop RH04-15. (B) Sketch of outcrop indicating the orientation of major structural features. (C) Block diagram illustrating the orientation of olivine axes in the dunite layer within the host rock of the shear zone. (D) Olivine LPO data from seven samples from the dunite layer within the host rock of the shear zone. The left column displays the LPO data relative to the foliation and lineation of the shear zone. The right column displays the LPO data relative to the foliation and lineation of the host rock. The contour interval on all equal area nets is 2.

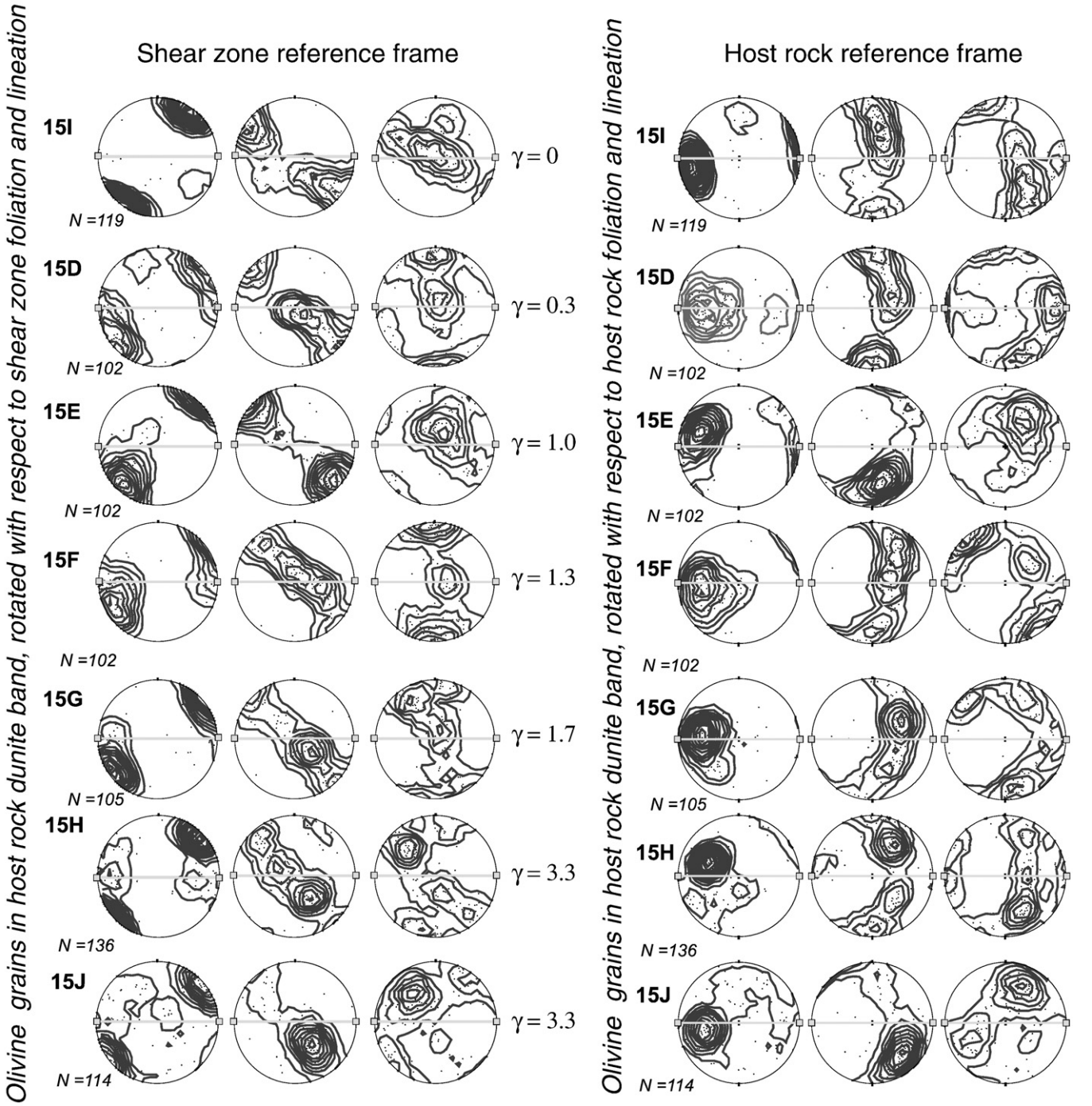

Fig. 10 (*continued*).

Table 1
Shear and finite strain measurements in shear zones at Red Hills.

Shear zone	Thickness (cm)	Offset	γ	S_1	S_2	R
RH04-9, Zone A	10	114	11.4	11.5	0.1	132.0
RH04-9, Zone B	2	10	5.0	5.2	0.2	27.0
RH04-12	8	44	5.5	5.7	0.2	32.2
RH04-15, Zone A	1	4	3.5	3.8	0.27	14.2
RH04-15, Zone B	1	52	52	52.0	0.02	2706.0
RH04-22A	4	7	2.0	2.4	0.4	5.9
RH04-22C, Zone A	2	17	11.3	11.4	0.1	130.4
RH04-22C, Zone B	2	75	50.0	50.0	0.0	2502.0

maximum perpendicular to host rock foliation and lineation. The [001] also form a diffuse girdle perpendicular to host rock foliation and lineation.

Table 2
Shear and finite strain measurements calculated from rotation of dunite layer in host rock in outcrop RH04-15. Angle (α) of unrotated layer is 120°.

Sample	α'	γ	S_1	S_2	R
15D	105	0.3	1.2	0.9	1.4
15E	68	1.0	1.6	0.6	2.6
15F	55	1.3	1.8	0.5	3.3
15G	42	1.7	2.2	0.5	4.6
15H	20	3.3	3.6	0.3	12.9

As strain increases toward the shear zone (Table 2), the patterns rotate. Olivine LPOs plotted relative to the shear zone foliation and lineation show that [100] become slightly more diffuse, and rotate toward the shear zone lineation. At $\gamma = 0.3$ (sample 15D), the [100] maximum has rotated from 55° from the shear zone lineation at $\gamma = 0$ (15I) to ~35° from the shear zone lineation. This orientation remains between 30° and 45° from the shear zone lineation as strain increases (Fig. 11). The two samples from immediately adjacent to the shear zone (15H and 15J), which show the highest strains ($\gamma = 3.3$; $R = 12.9$), show double maxima of [100] axes; the stronger maximum remains ~45° from the lineation, as in the lower strain samples, but the weaker maximum is approximately parallel to the lineation.

The angular width of the [100] (measured at 18 sigma) also changes from the lower strain samples to the higher strain samples. This angle increases to ~100° at $\gamma = 0.3$–1.7, but then decreases to ~60° at $\gamma = 3.3$. Interestingly, the trend in angular width of [100] changes in a manner consistent with variations in the angle between the [100] maxima and the lineation (Fig. 11). As the angles between the [100] maxima and the lineation decrease, the angular width formed by the [100] increases (Fig. 11).

The highest strain samples, $\gamma = 3.3$, (15H and 15J) contain double maxima. The stronger maximum in each of these samples is rotated away from the lineation relative to lower strain samples and has a narrower angular width formed by [100] (Fig. 11). The weaker maximum in these samples is parallel to the lineation.

[010] and [001] form more complicated patterns. As strain increases, [010] and [001] first concentrate in a point maximum, especially [010]. [010] remains more or less constant to higher strain. In the highest strain samples $\gamma = 3.3$, (15H and 15J), [010] form a diffuse girdle with a point maximum subperpendicular to the shear plane. [001] become increasingly diffuse with increasing strain and at high strain form a weak maximum subperpendicular to the shear plane.

In summary, with increasing strain, [100] rotate toward the lineation and, within the higher strain samples, exhibit double maxima. The highest strain samples (15H and J) contain a stronger concentration ~45° from the lineation, with a second, weaker concentration ~parallel to the lineation. [010] change little, while [001] become subperpendicular to the shear plane. The maximum angular width of [100] initially becomes broader. At high strain, double maxima are formed. The stronger maximum at ~45° from the lineation has a narrower angular width (~60°) than lower strain samples, and the weaker maximum is parallel to the lineation.

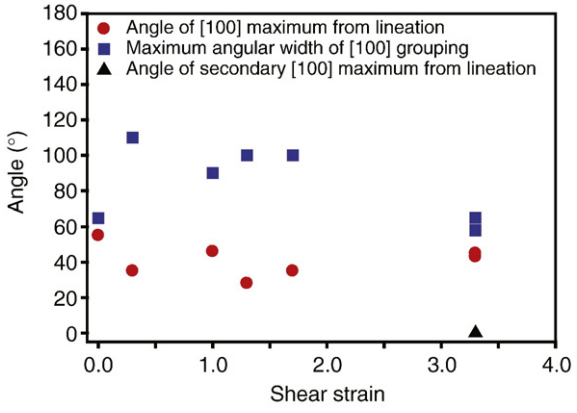

Fig. 11. Graph showing variations with shear strain of the angle between the [100] maximum and the lineation (circles) as well as the maximum angular width formed by groupings of [100] (squares). Note that decreases in the angle between the [100] and the lineation are complemented by increases in the maximum angular width. In the two highest strain samples ($\gamma = 3.3$), the angular width formed by [100] has decreased for the stronger maximum, but a weaker second maximum is parallel to the lineation (triangle).

4.6. Overview of olivine LPO data

The olivine LPO data collected from host rock and shear zones exhibit variability, yet four consistent patterns can be noted: First, when viewed in a geographic reference frame, olivine LPO in shear zones and host rocks are similar. Second, the olivine LPO in shear zone samples is more diffuse than the LPO in host rock samples, especially [001]. Third, for most shear zone samples, when viewed in a sample reference frame, some portion of [100] are approximately parallel to the lineation. [100] form double maxima, with one maximum parallel to the lineation and one maximum (similar to the host rock maximum when viewed in the geographic reference frame) perpendicular to the lineation (outcrops RH04-12 (Fig. 8D) and RH04-22A (Fig. 9D)). [100] also form girdles parallel to the plane of the shear zone (outcrop RH04-9 (Fig. 7D)), or rotate toward the lineation (outcrop RH04-15 (Fig. 10D)). Similarly, [001] are parallel to the lineation in outcrops RH04-9, RH04-12 and RH04-22 (Figs. 7–9, respectively), although [001] are diffuse and also show double maxima. Finally, olivine LPO in harzburgite host rock shows more diffuse patterns than olivine LPO in dunite host rock (outcrop RH04-9; Fig. 7).

5. Fourier transform infra-red analyses

Experimental work has suggested that water content may influence the activation of different slip systems (Jung and Karato, 2001a; Katayama et al., 2004; Jung et al., 2006). Fourier transform infra-red (FTIR) spectroscopic measurements were collected to determine the water content in the olivine in these Red Hills rocks.

5.1. FTIR methods

Infra-Red spectra were collected using a Nicolet Magna 560 FTIR spectrophotometer with NicPlan microscope (at Texas A&M University), employing an IR polarizer in the microscope. Doubly-polished thin sections (136–280 μm thick) were prepared from three sets of shear zone/host rock pairs from outcrops RH04-09 (RH3, 9C, and 9F), RH04-10 (10C and 10E), RH04-12 (12B and 12D). These sections were cut such that the majority of grains are oriented with one of the crystallographic axes perpendicular to the section plane. A total of 512 scans were collected for wavenumbers 650–4000 cm^{-1} at a resolution of 4 cm^{-1}. Each analysis area was 100 × 100 μm.

Although the rocks of the Red Hills are macroscopically unserpentinized, many 10–100 μm-wide fractures filled with serpentine cross-cut the olivine grains (Fig. 12A). Fracture-free areas with no obvious inclusions of fluid or serpentine were chosen for analysis. Unfortunately, many areas contain microscopic elongate inclusions of serpentine (Fig. 12B) that were detected by a large peak at 3688 cm^{-1} (Fig. 13; e.g. Fuchs et al., 1998; Matsyuk and Langer, 2004) that mask the peaks due to absorption from O–H bonds in olivine. No contamination due to the presence of epoxy was observed (peaks at 2852, 2922 and 2955 cm^{-1}).

Background subtraction was performed using the program described by Asimow et al. (2006). After background subtraction, most samples only contained the specific peaks due to water in olivine (3525, 3573, 3598 and 3611 cm^{-1}; Figs. 13 and 14A). However, in three samples a broad absorption band due to free water from 2800 to 3800 cm^{-1} was observed in addition to the peaks due to water in olivine (Fig. 15). For these samples, the free water contribution to the total water content was determined and subtracted from the spectra (Fig. 14A). The intracrystalline water content in olivine was then calculated by the same method as the rest of the samples described below.

Most studies of the water contents of deformed olivine aggregates and single crystals have used the method of Paterson (1982) for determining water concentrations in silicate glasses from unpolarized FTIR spectra. However, Bell et al. (1995, 2003) documented that this

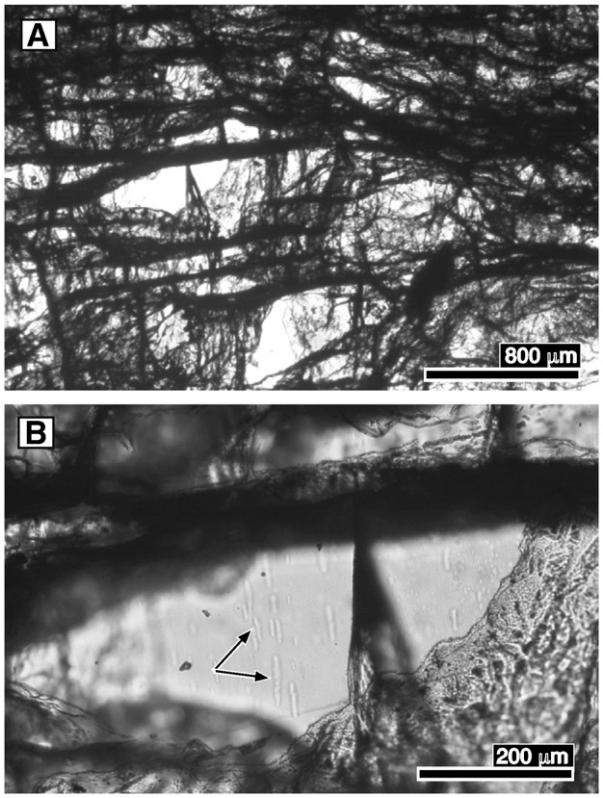

Fig. 12. Optical photomicrographs of (A) small-scale serpentine filled fractures and (B) inclusions of serpentine within a larger olivine grain.

method underestimates the water contents in silicate minerals such as olivine, garnet, orthopyroxene and clinopyroxene by a factor of 2–4 times the amount measured by independent methods. Bell et al. (2003) developed a new calibration for analyzing the water content in olivine based on the total absorbance of three separate spectra collected using polarized light. Each spectrum was collected from three individual sections from a single olivine crystal with either [100], [010] or [001] parallel to E (the vibration direction of the electric vector). This method is impractical for studies of water contents in small olivine grains because it requires three separate thin sections from a single grain of olivine.

Asimow et al. (2006) developed a method to determine the water content from the spectra collected from a minimum of three randomly oriented olivine grains using polarized light, and assuming that all of the individual grains measured have the same water content. However, several of our samples only have one grain that was uncontaminated by serpentine inclusions which made using the Asimow et al. (2006) method impossible.

Because the sections were cut perpendicular to a strong LPO of the sample, the olivine grains generally had one crystallographic axis perpendicular to the section plane. We used this information to create a calibration for single measurements based on the relative absorbances for principal spectra of known water content from Bell et al. (2003) and Asimow et al. (2006) methods. The relative contributions of the absorbance of each principal spectrum to the total absorbance from their spectra were calculated to be 70.7% (±13.1%) for *a*-axis parallel to E, 19.8% (±7.7%) for *c*-axis parallel to E, and 9.5% (±5.8%) for *b*-axis parallel to E. We recalculated the calibration of Bell et al. (2003), based on the relative contributions of the principal orientations to the total absorbance due to O–H stretching, with the limitation that only one measurement is possible but with a known orientation parallel to a principle axis. These recalculations are:

$$\text{ppm(wt)}H_2O = 0.188*(\text{Abs}_a + \text{Abs}_b + \text{Abs}_c)$$

$$\text{ppm(wt)}H_2O = 0.266*(\text{Abs}_a)$$

$$\text{ppm(wt)}H_2O = 0.947*(\text{Abs}_c)$$

$$\text{ppm(wt)}H_2O = 1.998*(\text{Abs}_b)$$

where Abs_x is the absorbance due to water in olivine from a spectrum normalized to the sample thickness in centimeters (Bell et al., 2003). This method is only appropriate if the orientation of the measured grain is close to the principal orientation, and the measured grain yields a spectrum with similar peaks and similar relative strengths of the peaks to the reference spectra collected from principal orientations.

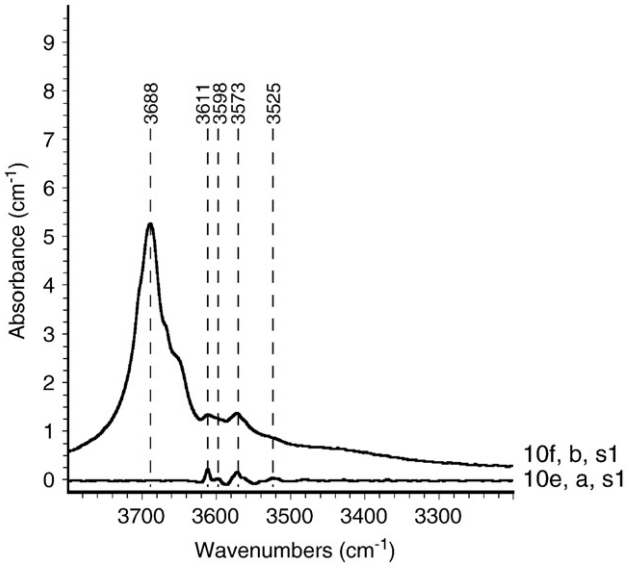

Fig. 13. FTIR spectra of olivine with microscopic serpentine inclusions (upper spectra with a large characteristic peak at 3688 cm^{-1}) and spectra of olivine with peaks due to O–H bonds only (lower spectra). See text for discussion.

5.2. FTIR results

Measurements of olivine grains that lack serpentine, talc and epoxy contamination (as judged by optical examination and lack of first-order absorption bands of secondary phases) were collected from samples 9F, RH3, 10E, 12B and 12D (Fig. 14). No measurements collected from samples 9C and 10F were free from contamination by serpentine or talc. In samples 9C and 10F, the relative strength of the water absorption band associated with serpentine and contamination was much greater than the peaks due to water in the olivine surrounding the small serpentine inclusions (Fig. 13). Therefore, these measurements were discarded.

The spectra collected from samples 9F-a-5, 12B-b-5 and 12D-b-4 contained a broad absorption band due to free water (Fig. 15). The water content due to free water was calculated by first determining the integrated absorption of the broad water band and then calculating the water concentration using a calibration for free water (A. Kronenberg, pers. comm., 2006). The free water contents in samples 9F-a-5, 12B-b-5 and 12D-b-4 are 134, 29 and 84 H/10^6 Si, respectively, and total water contents including both free and intracrystalline water are 185, 72 and 94 H/10^6 Si, respectively. The water associated with the broad absorption band is most likely due to sub-optical inclusions. It is possible that these inclusions represent intracrystalline water present during olivine deformation that has

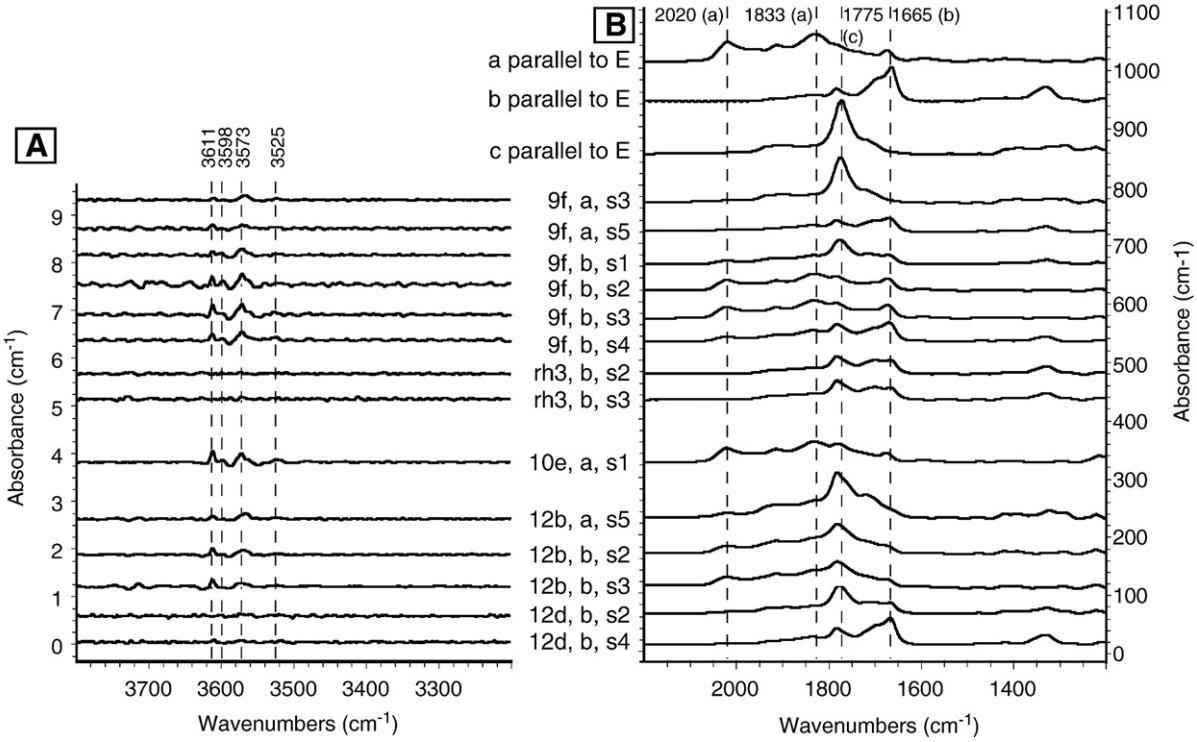

Fig. 14. FTIR spectra collected from samples 9F, RH3, 10E, 12B and 12D. All spectra are background subtracted and normalized to the sample thickness in cm. All spectra are offset for clarity. (A) Spectra in the region from 3200 to 3800 cm^{-1}. Most samples have very small absorbances at peaks located at 3525, 3575, 3598 and 3611. (B) Principal orientation spectra for sample GRR997 of Asimow et al. (2006) and from this study in the region from 1200 to 2200 cm^{-1}.

since exsolved. However, inclusions are not present in all samples, which may indicate that the micro-inclusions formed after deformation, possibly as a result of fluid infiltration along microcracks.

Integrated absorbances were calculated from spectra normalized to the thickness of the sample over the range of 3000 to 3800 cm^{-1}. Integrated absorbances range from 0.256 to 4.462 cm^{-2} (Table 3). The water contents of the olivine grains due to intracrystalline water in these samples range from 0.3 to 4.2 ppm (wt) (5 to 69 H/10^6 Si; Table 3). The average water content of the olivine grains in samples collected from shear zones was higher than the host rock at outcrop RH04-09, but was lower in the samples from outcrop RH04-12.

6. Discussion

6.1. Origin of olivine LPO in shear zones

Host rock LPO is generally consistent with {0*kl*}[100] slip (e.g., samples 15I, 12D, 9f, RH1), although [010] and [001] show some variations in orientation, with samples 9C and B and 12D suggesting (010)[100]. Experimental work predicts that the most common slip system likely to form in the upper mantle under dry conditions is the system (010)[100] (e.g., Kohlstedt and Goetze, 1974; Nicolas and Poirier, 1976; Durham and Goetze, 1977; Mercier, 1985; Bai et al., 1991; Bai and Kohlstedt, 1992; Hanson and Spetzler, 1994).

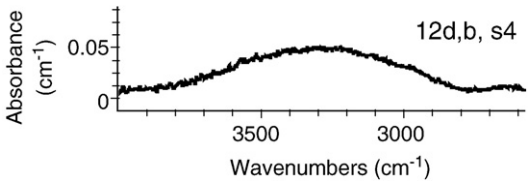

Fig. 15. FTIR spectra of sample 12d, section b, spot s4, which contains a wide band from 3000 to 3800 cm^{-1}, as is commonly attributed to "free" water in quartzites. See text for discussion.

Furthermore, many studies of naturally deformed rocks report evidence of the (010)[100] and {0*kl*}[100] slip systems in upper mantle rocks from settings such as mid-ocean ridges, island arcs, and mantle shear zones (e.g. Boudier and Coleman, 1981; Strotzki et al., 1990; Vissers et al., 1995).

In contrast with the host rock LPOs, many of the shear zone samples contain LPOs with a maximum of [100] perpendicular to the lineation and in the shear plane and, [010] subperpendicular to the shear plane and [001] at a low angle to the lineation (e.g., samples 9E, 9D, 9A and RH3 (Fig. 7); 12A and B (Fig. 8); and 22A1 and 22A2 (Fig. 9)). While double maxima are observed for [100] (e.g., samples 12A and 12B (Fig. 8) and 22A1 (Fig. 9)) and [001] (e.g., samples 12A and 12B (Fig. 8)), and [001] are often diffuse, the [100] maximum perpendicular to the lineation suggests possible slip on (010)[001], an atypical LPO for naturally deformed upper mantle rocks.

The interpretation of this LPO is complicated by a large number of experimental studies of olivine aggregates that produce this LPO under a wide range of conditions of pressures, temperatures, fluid content, melt content, and by different deformation mechanisms. The activation of the slip system (010)[001] has been attributed to 1) high stress/low temperature deformation in the presence of water (Jung and Karato, 2001a; Jung et al, 2006; Katayama and Karato, 2006; Karato et al., 2008); 2) deformation in the presence of melt (Holtzman et al., 2003); and 3) this LPO has formed by diffusion creep during experimental deformation of fine-grained aggregates of olivine and orthopyroxene deformed at low stresses (Sundberg and Cooper, 2008). Slip on [001] has also been identified in rocks experimentally deformed at low temperatures (e.g., Carter and Ave'Lallemant, 1970). However, it is unlikely that significant ductile strains will accumulate at these low temperatures. High pressure deformation experiments of olivine single crystals (Raterron et al., 2009) and aggregates (Couvy et al., 2004; Raterron et al., 2009; Jung et al., 2009) have suggested that high pressures may also be responsible for a transition to (010)[001] glide. However, the pressures under which these experiments were carried out (~3 GPa; Jung et al., 2009 to 8.5 GPa; Raterron et al., 2009)

Table 3

Sample	Section	Spot	Section thickness (mm)	Integrated absorbance (cm^{-1})	Axis parallel to E	Conversion factor	H_2O ppm (wt)	$H/10^6$ Si
9f	a	3	263	3.24	*c*	0.95	3.1	50
9f	a	5	263	1.56	*b*	2	3.1	51
9f	b	1	136	2.44	*c*	0.95	2.3	38
9f	b	2	136	2.49	*a*	0.27	0.7	11
9f	b	3	136	3.59	*a*	0.27	1.0	16
9f	b	4	136	4.46	*c*	0.95	4.2	69
9f avg							2.4	39
9f calculated from synthetic spectra				7.65		0.19	1.4	23
rh3	b	2	220	0.3	*c*	0.95	0.3	5
rh3	b	3	220	0.76	*c*	0.95	0.7	12
10e	a	1	258	3.17	*a*	0.27	0.8	14
12b	a	5	280	2.31	*c*	0.95	2.2	36
12b	b	2	155	2.68	*c*	0.95	2.5	41
12b	b	3	155	2.74	*c*	0.95	2.6	42
12b avg							2.4	40
12b calculated from synthetic spectra				6.58		0.19	1.2	20
12d	b	2	172	1.41	*c*	0.95	1.3	22
12d	b	4	172	0.26	*b*	2	0.5	8

are substantially higher than the pressures estimated for the Red Hills deformation (~1 GPa; Webber et al., 2008).

Studies of naturally deformed rocks have reported this LPO as well (Newman et al., 1999; Mizukami et al., 2004; Skemer et al., 2006). In these field-based studies, Mizukami et al. (2004) and Skemer et al. (2006) attribute the development of the LPO to the presence of water, although only Mizukami et al. (2004) present microstructural evidence for the presence of water during deformation. Newman et al. (1999) report the development of a weak olivine LPO of this type in fine-grained aggregates of olivine and orthopyroxene, and suggest that it formed during grain boundary sliding or diffusion creep.

Also related to the observations of the Red Hills shear zone samples are the results of Michibayashi and Mainprice (2004) from naturally deformed rocks, which suggest that modification of a pre-existing LPO activates atypical slip systems. Below, we discuss hypotheses 1–3, above, as well as the possibility that a pre-existing LPO influenced the formation of the unusual LPOs in the small-scale shear zones at Red Hills.

6.1.1. Olivine LPO developed in the presence of water?

Previous workers have demonstrated that water influences the deformation mechanisms and grain size in olivine (Carter and Ave'Lallemant, 1970; Chopra and Paterson, 1981, 1984; Mackwell et al., 1985; Karato et al., 1986; Mei and Kohlstedt, 2000a,b; Jung and Karato, 2001a,b). Furthermore, experimental results of olivine deformation indicate that the presence of water affects the operative slip systems (Mackwell et al., 1985).

Jung and Karato (2001a), Katayama et al. (2004), Jung et al. (2006), Katayama and Karato (2006), and Karato et al. (2008) describe olivine slip systems that are activated at varying water levels and stress and temperature conditions. Jung and Karato (2001a) identify two slip systems, "Type-B" and "Type-C," in which [001] axes form concentrations subparallel to the shear direction. [001] that are subparallel to the shear direction are identified in recent studies of naturally deformed peridotites (e.g. Frese et al., 2003; Mizukami et al., 2004). Both Mizukami et al. (2004) and Frese et al. (2003) interpret the LPO patterns they measure to be the result of deformation in the presence of water.

The FTIR results for the Red Hills rocks suggest that neither the shear zone nor the host rock samples contain large amounts of water. All measured water contents were considerably less than the amount cited by Jung and Karato (2001a) and Katayama et al. (2004) necessary to cause a switch from (010)[100] slip (type A) to (001)[100] slip (type E, $300 > c_H > 800$ $H/10^6$ Si) or (100)[001] slip (type C, $c_H > 800$ $H/10^6$ Si). Additionally, the measured water contents are not systematically higher in the samples from shear zones than the water contents measured from samples of the adjacent host rock.

The grain size (>1 mm) in the Red Hills shear zones is similar to the grain size observed in the host rock. The large grain size in the shear zones, despite the evidence for high strain, could indicate enhanced recovery rates associated with the presence of water in shear zones during deformation and subsequently lost from the system. However, in contrast to the water-related microstructures reported by Mizukami et al. (2004), only rare micro-inclusions in olivine grains were observed in the Red Hills shear zones.

Alternatively, the large grain size, straight grain boundaries, and numerous 120° triple junctions may result from later annealing or static recrystallization. Experimental evidence from deformed and statically annealed quartzites shows that annealing does not obliterate the LPO, but does cause microstructures similar to those observed in the Red Hills shear zones (Heilbronner and Tullis, 2002).

6.1.2. Olivine LPO developed in the presence of melt?

Holtzman et al. (2003) describe an olivine LPO pattern in which [001] axes form a concentration parallel to the shear direction and (010) is parallel to the shear plane. They suggest that when melt segregates into bands that are oriented ~20° from clockwise from the shear plane with a right lateral sense of shear, the orientation of [100] and [001] axes are switched. The LPO pattern is similar both inside and outside of the melt-rich bands.

It is appealing to apply these results to the Red Hills data, because it could potentially explain the similarity in orientation of olivine LPO inside and outside of the shear zones. However, it is unlikely that the formation of the shear zones was synmagmatic. The boudinage of pyroxenite dikes within dunite shear zones (e.g., samples 12 and 22A) indicate that the deformation within the shear zones occurred in the solid state. The cross-cutting orthopyroxenite dikes must postdate the formation of the dunite bands. The boudinage and displacement of the orthopyroxenite dikes indicate that they were present prior to the deformation along the shear zones, and that the dikes were in the solid state prior to deformation. In addition, if the LPOs in the shear zones are melt related, the orientation of the shear zones might be expected to dip ~20° from the (010) axis in the direction of shear (e.g. SW). Instead, shear zones dominantly dip to the SE (082 35° SE). Further, if the shear zones were formed by shear localization in the presence of melt, the lineations in both the shear zones and host rocks should be parallel to [001] axes, but this is not observed in the Red Hills samples. In support of these geometric arguments, no melt-related mesoscopic structures or microstructures were observed in the Porter's Knob area. Finally, temperatures calculated for Red Hills

shear zone compositions are generally the lowest recorded in the field area (Webber, 2005), a result that is inconsistent with a melt-related hypothesis.

6.1.3. Olivine LPO developed as a result of grain boundary sliding?

Sundberg and Cooper (2008) deformed fine-grained (~2–5 μm) olivine–orthopyroxene aggregates at low (<20 MPa) stresses and observed an olivine LPO consistent with (010)[001] slip. However, only rare dislocations were observed and the olivine flow law of Hirth and Kohlstedt (2003) predicts diffusion creep for their experimental conditions ($d = 0.002$–0.005 mm, 1200 °C, 1.6 GPa confining pressure, shear strain rate $\sim 2\times10^{-4}$/s). Sundberg and Cooper (2008) suggest that their samples deformed by diffusion-accommodated grain boundary sliding and that the LPO developed as a result of easier sliding on some crystallographic planes than on others.

We infer that the olivine grains in the Red Hills are not deforming by a grain boundary sliding mechanism, such as inferred in the Sundberg and Cooper (2008) experiments. First, the conditions of deformation in the Red Hills ($d = 2$–5 mm, $T \approx 749$–1000 °C, $P \approx 1$ GPa, assuming a strain rate of 1×10^{-13}/s to 1×10^{-15}/s, $C_{OH} = 0$–1000 H/10^6 Si)) are consistent with conditions necessary for dislocation creep, as predicted by the flow law for olivine of Hirth and Kohlstedt (2003) (Fig. 16). Second, the gradual rotation of the [100] maximum, with increasing strain, in samples from RH04-15 (Fig. 10), suggest that dislocation activity continued with increasing strain. This result is inconsistent with a grain boundary sliding mechanism.

6.1.4. Olivine LPO as a result of a pre-existing fabric?

The similarity in olivine LPOs between the host rock and shear zone samples, when viewed in the geographic reference frame, suggests that the dunite zones contained the same LPO as the surrounding host rocks prior to their activation as shear zones. During shear, this pre-existing LPO was modified, but not completely reset. For example, samples 9E and D of shear zone A in RH04-9 (Fig. 7) have a similar olivine LPO to the host rock samples in that exposure, when viewed in the geographic reference frame. When viewed in the shear zone reference frame, olivine [100] axes of 9E and D are within the shear zone plane and perpendicular to the lineation. Thus, the olivine LPO may not indicate (010)[001] slip, but rather, is a remnant of a pre-existing LPO. Likewise, the double maxima evident in some samples (e.g. outcrops RH04-12 and 22 (Figs. 8 and 9) may contain one maximum that is a remnant of an initial LPO, while the second maximum formed during the shear zone deformation.

The second maximum of [100] is commonly at a low angle to the lineation (e.g. samples 12A, 22A1, 15H and J (Figs. 8–10)) or forms a weak girdle parallel to the plane of the shear zone (e.g. samples 9A and RH3 (Fig. 7)). [001] tend to be diffuse and at a low angle to the lineation (e.g., outcrops 9 and 22A (Figs. 7 and 9)) but are also observed perpendicular to the lineation in the shear plane (e.g., samples 12A and B (Fig. 8)). These orientations suggest that (010)[100] or {0*kl*}[100], more typical slip systems for dry upper mantle rocks, were active during deformation along these shear zones.

Two studies report on the influence of a pre-existing LPO on the development of LPO during shear zone deformation in two sections of

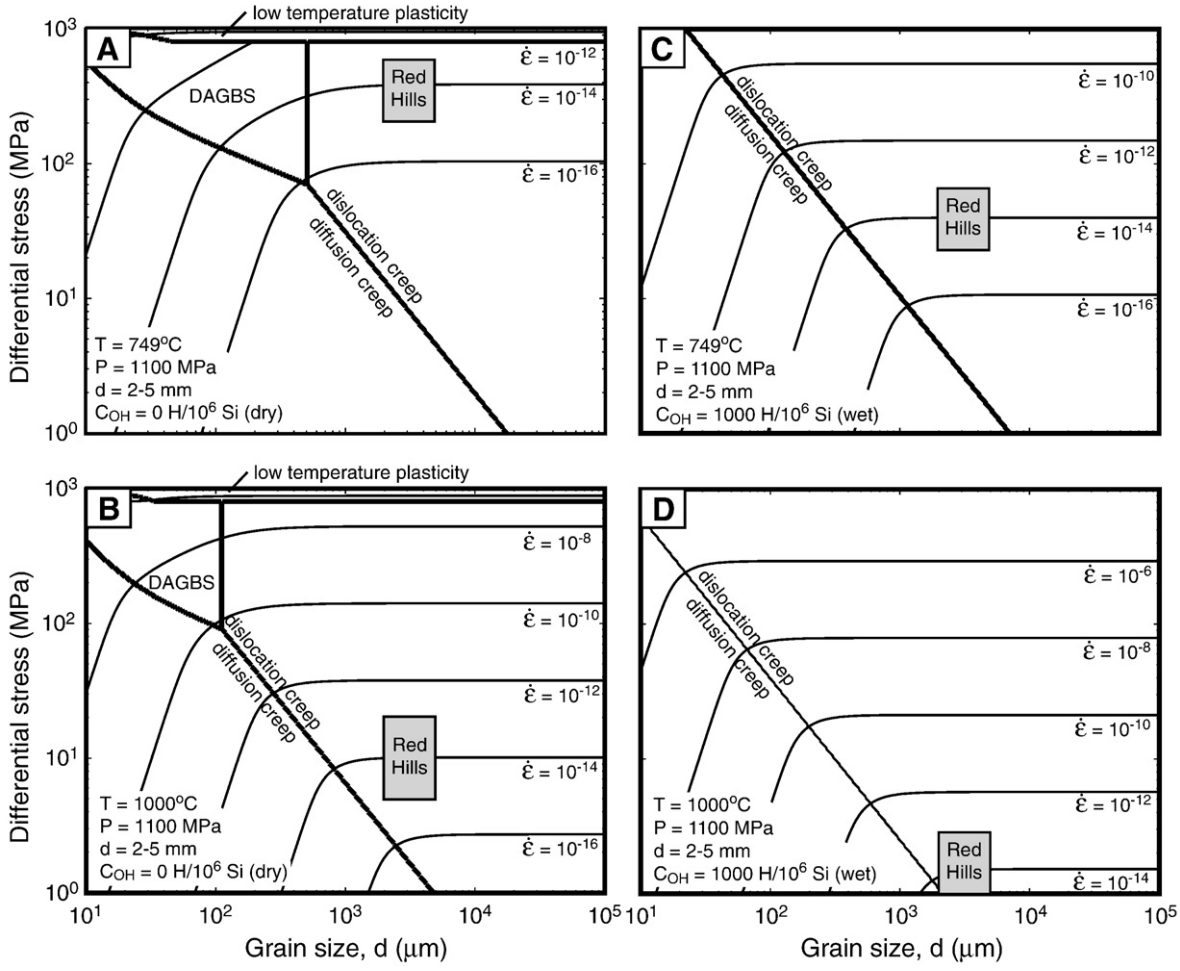

Fig. 16. End-member deformation mechanism maps for olivine at the Red Hills, NZ calculated for low (749 °C; A, C) and high (1000 °C; B, D) temperatures and reasonable ranges of water contents (0 H/10^6 Si; A, B and 1000 H/10^6 Si; C, D) using the Hirth and Kohlstedt (2003) flow law for olivine aggregates. The grey box indicates the probable range of conditions for the Red Hills and is defined by the grain size (2–5 mm) and natural strain rates (10^{-13}/s–10^{-15}/s).

the Oman Ophiolite (Hilti massif: Michibayashi and Mainprice, 2004; Fizh massif: Michibayshi et al., 2006). Michibayashi and Mainprice (2004) suggest that a pre-existing LPO in the Hilti massif resulted in the activation of an unusual slip system for the upper mantle, (001)[100]. Interestingly, [010] retained its geographical orientation during the later deformation event. In the Fizh massif, Michibayshi et al. (2006) record the evolution of LPO associated with a similar rotation of foliation and lineation as observed in the Hilti Section, but document little change in the operative slip system ({0*kl*}[100]). While the slip system remained the same, the geographic orientation of the axes did change with the change in foliation and lineation.

While the Red Hills shear zones retain some evidence of the pre-existing LPO, similar to the Michibayashi and Mainprice (2004) observations, there is at least one difference. The preferential slip system activated in the Red Hills shear zones appears to be (010)[100], a common slip system for upper mantle rocks. Consequently, the scenario is perhaps more similar to the Fizh shear zone rocks (Michibayshi et al., 2006). It is not clear if this LPO influenced the dominant slip system during shear zone deformation.

The Red Hills also differ from the above examples in that the dunite shear zone rocks are a different lithology from the host rock (banded harzburgite), with a sharp boundary between the two. The location of the pre-existing dunite bands likely controlled the location of the shear zones, placing greater constraints on the location and transport direction in these rocks than in the shear zones discussed in Michibayashi and Mainprice (2004) and Michibayshi et al. (2006).

An alternative explanation to incomplete resetting of LPO, is that the similarity in the geographic orientation of olivine LPO in shear zone and host rocks results from a later deformation event. This hypothesis would also account for the similarity in microstructures (e.g. coarse grain size and abundant polygonal grains) in both shear zones and host rock. However, the regional geology of the Porter's Knob area (Webber et al., 2008) suggests that the Central Domain compositional foliation is the earliest formed fabric in the area. In addition, the variation in temperatures calculated by geothermometry does not support a later deformation event. Webber (2005) reports that while calculated temperatures are variable, both on the scale of a thin section and among different samples with similar fabrics, shear zones record some of the lowest temperatures in the region. Resetting of the olivine LPO during a later event is also contradicted by the systematic rotation of LPO observed in the dunite band rotated by a shear zone in outcrop RH04-15 (Fig. 10).

6.2. Evolution of LPO with strain

The incomplete resetting of the orientations of the axes that we observe in these shear zones, at the high shear strains recorded ($\gamma = 2$–11.4; Table 1), is inconsistent with results from simple shear deformation experiments of synthetic olivine aggregates, with random starting LPO, that indicate strains of $\gamma \sim 1.0$–2.0 necessary to form a LPO (defined as [100] parallel to the flow direction (Zhang and Karato, 1995; Zhang et al., 2000; Bystricky et al., 2000)). Numerical simulations (viscoplastic self-consistent (VPSC) models) predict that [100] maximum approaches the flow direction at $\gamma < 1.5$ (Tommasi, 1998; Tommasi et al., 2000).

A problem with direct comparison between LPOs observed in these modeling and experimental studies to those observed in the Red Hills is that the modeling and experimental studies started with randomly oriented grains, whereas the Red Hills had a pre-existing LPO. Warren et al. (2008) similarly found that naturally sheared harzburgites from the Josephine Ophiolite, which also contained a pre-existing LPO, required somewhat higher strains to reset LPOs than predicted by experiments and models. The Josephine shear zone rocks required $\gamma = 2.58$ before [100] were parallel to the flow direction (Warren et al., 2008).

Higher strains, however, are recorded in the Red Hills shear zones than in the Josephine shear zone without complete resetting of the LPO. Significantly, in the Red Hills shear zones, there is no consistent relationship between the amount of finite strain or shear strain in an individual shear zone and the LPO orientation or intensity. For example, the higher strain samples (e.g., 9A; Fig. 7, $\gamma = 11.4$) do not necessarily show greater variation in LPO from the host rock than the lower strain samples (e.g., 22A; Fig. 9; $\gamma = 2.0$). We do observe minor variations in LPO between samples from the same shear zones, suggesting that the discrepancy between our results and the experiments and models may be, in part, a result of heterogeneous strain within the natural dunite shear zones. This heterogeneity, combined with our observations from separate shear zones that may have experienced different deformation histories, make a direct comparison with other studies difficult.

6.2.1. Evolution of LPO within a strain gradient

The dunite band (outcrop RH04-15) that is rotated into parallelism with a cross-cutting shear zone, provides an ideal opportunity to investigate the development of LPO with strain by considering changes in LPO within a strain gradient. Within the host rock sample (15I; $\gamma = 0$), [100] are 55° from the shear zone lineation. As shear strain increases to $\gamma = 0.3$, [100] rotate toward the flow direction (35° from the lineation), and the angular width formed by [100] increases (from 68° to 110°) (Fig. 11). Interestingly, as the angle between the [100] maxima and the lineation decreases, the angular width formed by [100] increases (Fig. 11). Within the high strain samples, $\gamma = 3.3$, double maxima are observed. The stronger maximum has an increased angle from the lineation (45°), but the weaker maximum is parallel to the lineation (Fig. 10). The data from RH04-15 suggest that the wide angular width formed by [100] in the lower strain samples ($\gamma = 1.0$–1.7) may reflect the initial development of [100] parallel to the lineation. Experimental deformation of olivine in shear has formed similar bimodal peaks of [100], with one peak parallel to the lineation, and a second at 45° to 60° to the lineation (Bystricky et al., 2000; Zhang et al., 2000; Lee et al., 2002).

It is interesting to note that in RH04-15, the bulk of the [100] remain at a high angle (45°) to the lineation. The LPO has been modified, but not entirely reset during shear strain, similar to our observations from the individual dunite shear zones, described above.

Warren et al. (2008) studied a similar reorientation of olivine LPO with increasing strain associated with a shear zone in harzburgites, and their results are comparable to the LPOs reported for the dunite band described here. The harzburgites described by Warren et al. (2008) also contain a pre-existing LPO (with [100] 62° from the shear zone lineation; [010] and [001] differ from those reported in RHO4-15). They also note an initial rotation of [100] axes toward the lineation (at $\gamma = 0.65$, the lowest strain they report.) At high strains, however, they do not report double maxima. Rather at $\gamma = 2.58$, [100] are parallel to the flow direction (Warren et al., 2008).

In both of these studies of naturally deformed shear zone rocks with pre-existing LPOs, higher strains are required for [100] to be parallel to the flow direction than predicted by experiments and numerical models that begin with random olivine aggregate orientations. The initial rotation of [100] in the natural samples toward the flow direction, however, occurs at low strains. The RH04-15 dunite shear zone records a rotation of [100] toward the shear zone flow direction at only $\gamma = 0.3$. The orientation of [010] remains stable to high strains, while [001] gradually rotate so that they are sub-perpendicular to both the lineation and the shear plane (Fig. 10). The orientation of the pre-existing LPO likely influences the initial slip system (c.f. Warren et al., 2008).

A striking difference between the Red Hills and Josephine outcrops is the magnitude of shear strain required to reorient [100]. Warren et al. (2008) report olivine [100] parallel to the lineation in the Josephine harzburgites at $\gamma = 2.58$. In contrast, the dunite described here only

contains a weak, secondary maximum parallel to the lineation, with most [100] axes 45° from the lineation, at $\gamma = 3.3$. Possible explanations for this difference include different lithologies (harzburgite vs. dunite), different starting LPOs requiring different amounts of shear strain to reset the orientations of [100], or the activation of different slip systems or mechanisms of recrystallization (Zhang et al., 2000; Lee et al., 2002). With the available evidence, we are not able to determine which of these explanations, or combinations of explanations, are responsible for the observed differences in LPO between the Josephine shear zone and the shear zone from RHO4-15.

6.3. Comparison between harzburgite and dunite host rock LPO

In shear zone RH04-9 (Fig. 7), it is possible to compare LPOs between dunite and harzburgite samples that experienced similar deformation histories. Samples were obtained from a host rock dunite band (RH1 and RH2) that is parallel to the host rock foliation within the harzburgite. Samples were also obtained from the harzburgite host rock (9C and 9B) approximately 10 cm from the dunite band, and across the strike of the foliation. Sample locations RH2 and 9B are located 2 cm above a cross-cutting dunite shear zone, while RH1 and 9C are 20 and 24 cm above the shear zone, respectively. In spite of the proximity of the dunite and harzburgite samples, the olivine LPOs show some variations. Most obvious is a slight difference between the orientations of maxima in the dunite and harzburgite, especially 9B compared to RH2 (Fig. 7). The difference may be a result of strain partitioning between the rocks with different rheologies, although field investigations have suggested that up to 15% orthopyroxene in olivine-rich rocks does not affect the relative viscosity (Tikoff et al., in review). In addition, dunite samples yield girdles of [010], while the harzburgite samples more closely approximate point maxima. [001] are also more diffuse in the harzburgite samples than in the dunite samples, which may be a result of interactions with orthopyroxene grains within the harzburgite rocks.

Warren et al. (2008) similarly compared LPOs in naturally sheared harzburgite and dunite, and we note a few interesting contrasts between their observations and those described here. First, Warren et al. (2008) saw no change in the orientation of the LPOs for each axis between the harzburgites and dunites, while we note a slight variation. In addition, they note that [010] and [001] in the dunite sample studied ($\gamma = 3.86$) contain single maxima, while the harzburgite LPOs yield girdles. This observation is opposite the result reported here, where dunite samples (Fig. 7C; 9F and RH1 and RH2) yield girdles of [010] and [001] while harzburgites (Figs. 7C and 9C and B) more closely approximate single maxima.

In the samples Warren et al. (2008) studied, olivine within harzburgite domains has a finer grain size than adjacent dunite domains, leading Warren et al. (2008) to suggest that the difference in LPO resulted from dislocation creep accommodated grain boundary sliding in the harzburgite samples. Interestingly, in the samples from the Red Hills, where we report different LPOs, we note no difference in the grain size of olivine between harzburgites and dunites. This difference may reflect either no difference in the contribution from grain boundary sliding between the two domains or partial annealing resetting grain size.

6.4. Model for shear zone development

Shear zones in the Red Hills develop at a high angle to the host rock foliation, in a south-dipping orientation. The dunite shear zones are also characterized by coarse (>1 mm), polygonal grains, similar in size to host rock grains, that display complex LPO patterns. Mesoscopic and microscopic scale structures, geothermometry and FTIR are inconsistent with localization in the presence of water or melt. The pre-existing, cross-cutting, dunite and pyroxenite zones at Red Hills likely acted as heterogeneities that localized deformation within or adjacent to these zones.

We propose a four-step process for the formation of the shear zones. First, a foliation and compositional banding developed in the host rock, associated with the development of an LPO consistent with {0*kl*}[100] or (010)[100]. Second, dikes and/or melt-rock reaction zones (e.g., dunites represent former magma channels in which pyroxenes have been dissolved, after the model of Kelemen and Dick, 1995) are formed (tabular zones), in the absence of deformation, and in a range of orientations (Fig. 5). Third, if the tabular zones are of a replacive origin (e.g., Kelemen and Dick, 1995), they may have inherited the pre-existing LPO of olivine grains. Alternatively, the tabular zones and host rocks may have experienced a continuing or subsequent deformation that imparted an olivine LPO to the tabular zones and the surrounding host rock. Fourth, tabular zones that are ~EW-striking and S-dipping in orientation localize south-dipping shear zones, presumably because these tabular zones are in an orientation favorable for shear. Equilibrium textures suggest that this last stage was likely followed by partial annealing.

The interpretation of subsequent deformation localized along the shear zones is supported by the following observations: First, the boudinage of pyroxenite dikes within dunite shear zones (Figs. 8 and 9) strongly suggests that deformation took place in the solid state. Second, south-dipping shear zones have a range of compositions (i.e., dunite, pyroxenite and olivine websterite). Many tabular zones (e.g., dikes as well as bands within the harzburgitic host rock) throughout the Central Domain have similar compositions and thicknesses as the shear zones. Yet, only structures that are south-dipping are activated as shear zones with visible offset of host rock compositional banding. Third, olivine LPO within a host rock dunite layer shows systematic rotation with increasing strain as the layer is rotated into parallelism with a shear zone (Fig. 10). Finally, this interpretation is consistent with the larger-scale (50 m thick) south-dipping zone observed in the western portion of the Central Domain (Webber et al., 2008).

6.5. Implications

The implications of the Red Hill shear zone rocks for understanding mantle rheology include: 1) The role of compositional heterogeneity in the mantle in causing strain localization; 2) the influence of pre-existing LPO on texture development; and 3) a potential difficulty in interpreting mantle flow directions from interpretations of shear wave splitting data.

1) The Red Hills shear zones suggest that strain partitioning occurs in the lithospheric mantle at pressure and temperature conditions that characterize upper mantle deformation. In particular, strain is localized by zones of heterogeneous composition, including tabular dunite zones and thin pyroxenite bands. The observation of opposite sense of offset on dunite zones with minor differences in orientation (<20°) suggests that this strain partitioning effect is quite strong. This result is in contrast to ongoing work by our group in the Twin Sisters ultramafic body, USA, in which no variation of strain is observed in banded dunite/harzburgite (Tikoff et al., in review). The reason for this discrepancy needs to be resolved.
   One possible cause of the strain partitioning is that the sharp interface between wall rock and dike (dunite or pyroxenite) may have acted as a surface for strain localization, particularly if the dike was well oriented for deformation. Strain localization along lithological interfaces is documented in analog experiments (e.g., Ghosh and Ramberg, 1976) and in crustal rocks undergoing crystal-plastic deformation (e.g., Sengupta, 1997; Waters-Tormey and Tikoff, 2007).
2) Olivine LPO is not easily reset by deformation. The similarity in host rock and shear zone samples can most easily be explained by the influence of the pre-existing LPO on the development of shear

zone LPOs. The pre-existing LPO was not completely reset by subsequent deformation. Therefore, in order to interpret the dominant slip systems in the shear zone olivine, both host rock and shear zone LPO must be considered. This information can be evaluated in field studies by considering the LPO of deformed and host rocks within multiple reference frames. In cases where this approach is not possible — e.g., dunite xenoliths — slip systems evaluated solely from the xenolith fabric may be indeterminable.

3) Using LPO to infer flow patterns in the mantle may be complicated by overprinting deformations. Certainly, the shear zones in the Red Hills area are too small to be observed by geophysical techniques, such as shear wave splitting. However, our study does indicate that large strain values are required to reset a pre-existing LPO. If large-scale tectonic deformation of the lithospheric mantle acts over large areas, the displacement will inherently lead to lower strain values. Strain partitioning, discussed above, will require even larger deformations to reset the bulk fabric of the lithospheric mantle. Therefore, ongoing deformation may not be able to reset fossil anisotropy from earlier tectonic events. Fossil anisotropy may, therefore, have a major influence on mantle textures and observed seismic anisotropy.

7. Conclusions

South-dipping, cm-scale shear zones of dunite, pyroxenite and olivine websterite cross-cut banded dunite and harzburgitic host rock. The shear zones exhibit microstructures similar to the host rock, including a coarse (2–5 mm) grain size and dominantly polygonal grains. Host rock LPOs suggest the {0*kl*}[100] and/or (010)[100] slip system, common in naturally deformed upper mantle rocks, was active. In contrast, shear zone olivine LPOs, while frequently exhibiting double maxima and diffuse maxima, suggest (010)[001], an atypical slip system in the upper mantle.

While experimental deformation of olivine aggregates has produced the (010)[001] under different conditions (e.g., Jung and Karato, 2001a; Jung et al., 2006; Holtzman et al., 2003 and Sundberg and Cooper, 2008), these conditions have been determined to be unlikely in the Red Hills shear zones: FTIR analyses of shear zone and host rock samples indicate that neither the shear zone nor the host rock olivines are fluid-rich. Microstructures are inconsistent with the presence of fluids or melt, and mesoscopic-scale boudinage of pyroxenite dikes within shear zones indicate that shear zone deformation took place in the solid state. Deformation by grain boundary sliding is inconsistent with the coarse grain size in these shear zones, as well as with the gradual rotation of LPO in sample RH04-15, which suggests deformation by dislocation creep within a strain gradient.

When viewed in a geographic reference frame, host rock and shear zone LPOs are similar. The olivine LPO in shear zones is interpreted to reflect a pre-existing LPO that formed during the deformation event that formed the host rock LPO. The poorly clustered data and double maxima reflect the change during deformation along the shear zone. [100] at a low angle to the transport direction, and [001] at a high angle to both the shear zone plane and lineation suggest that shear zone deformation was dominated by (010)[100] slip.

This work suggests that olivine LPOs of shear zone rocks are significantly affected by pre-existing LPO and that strain partitioning along compositional domains occurs at least locally at mantle conditions.

Acknowledgements

Special thanks to Gordon Medaris for providing helpful insights into the petrology and microstructures of the Red Hills field area and to Andreas Kronenberg for his assistance and advice regarding the FTIR analyses. Laurel Goodwin is gratefully acknowledged for reading an early version of this manuscript. Thanks to Carrie Larson and Angela Hull for providing assistance in collecting olivine LPO data, and to Jessica Warren for sharing her MATLAB script for deformation mechanism maps with us. We thank two anonymous reviewers for their comments, which helped clarify aspects of the work and raised additional avenues to explore. This project was financially supported by the National Science Foundation (EAR 0409522 and EAR 0409567) and the Packard Foundation.

References

Asimow, P.D., Stein, L.C., Mosenfelder, J.L., Rossman, G.R., 2006. Quantitative polarized infrared analysis of trace OH in populations of randomly oriented mineral grains. American Mineralogist 91 (2–3), 278–284.

Bai, Q., Kohlstedt, D.L., 1992. High-temperature creep of olivine single crystals; 2, dislocation structures. Tectonophysics 206, 1–29.

Bai, Q., Mackwell, S.J., Kohlstedt, D.L., 1991. High-temperature creep of olivine single crystals 1. Mechanical results for buffered samples. Journal of Geophysical Research 96, 2441–2463.

Bai, Q., Jin, Z.-M., Green II, H., 1997. Experimental investigation of the rheology of partially molten peridotite at upper mantle pressures and temperatures. In: Holness, M.B. (Ed.), Deformation-enhanced Fluid Transport in the Earth's Crust and Mantle. Chapman and Hall, London, pp. 40–61.

Bell, D.R., Ihinger, P.D., Rossman, G.R., 1995. Quantitative analysis of trace OH in garnet and pyroxenes. American Mineralogist 80 (5–6), 465–474.

Bell, D.R., Rossman, G.R., Maldener, J., Endisch, D., Rauch, F., 2003. Hydroxide in olivine; a quantitative determination of the absolute amount and calibration of the IR spectrum. Journal of Geophysical Research 108 (2), 2105–2114.

Boudier, F., Coleman, R.G., 1981. Cross section through the peridotite in the Samail ophiolite, southeastern Oman Mountains. Journal of Geophysical Research 86, 2573–2592.

Boudier, F., Ceuleneer, G., Nicholas, A., 1988. Shear zones, thrusts and related magmatism in the Oman ophiolite: initiation of thrusting on an oceanic ridge. Tectonophysics 151, 275–296.

Boullier, A.M., Gueguen, Y., 1975. SP-mylonites — origin of some mylonites by superplastic flow. Contributions to Mineralogy and Petrology 50, 93–104.

Brey, G.P., Köhler, T., 1990. Geothermobarometry in four-phase lherzolites II. New thermobarometers, and practical assessment of existing thermobarometers. Journal of Petrology 31, 1353–1378.

Bystricky, M., Kunze, K., Burlini, L., Burg, J.-P., 2000. High shear strain of olivine aggregates: rheological and seismic consequences. Science 290, 1564–1566.

Carter, N.L., Ave'Lallemant, H.G., 1970. High temperature flow of dunite and peridotite. Geological Society of America Bulletin 81, 2181–2202.

Chopra, P.N., Paterson, M.S., 1981. The experimental deformation of dunite. Tectonophysics 78, 453–473.

Chopra, P.N., Paterson, M.S., 1984. The role of water in the deformation of dunite. Journal of Geophysical Research 89, 7861–7876.

Christensen, N.I., 1984. The magnitude, symmetry and origin of upper mantle anisotropy based on analyses of ultramafic tectonites. Geophysical Journal of the Royal Astronomical Society 76, 89–111.

Couvy, H., Frost, D.J., Heidelbach, F., Nyilas, K., Ungár, T., Mackwell, S., Cordier, P., 2004. Shear deformation experiments of forsterite at 11 GPa–1400 °C in the multianvil apparatus. European Journal of Mineralogy 16, 877–889.

Davis, T.E., Johnston, M.R., Rankin, P.C., Stull, R.J., 1980. The Dun Mountain Ophiolite Belt in East Nelson, New Zealand. Proceedings, International Ophiolite Symposium. Cyprus Ministry of Agriculture and Natural Resources, Nichoisa, Cyprus, pp. 480–498.

Dijkstra, A.H., Drury, M.R., Vissers, R.L.M., Newman, J., 2002. On the role of melt–rock reaction in the mantle shear zone formation in the Othris Peridotite Massif (Greece). Journal of Structural Geology 24, 1431–1450.

Dijkstra, A.H., Drury, M.R., Vissers, R.L.M., Newman, J., Van Roermund, H.L.M., 2004. Development of shear zones in mantle rocks: Evidence from alpine and ophiolitic peridotite massifs. In: Alsop, G.I., Holdsworth, R.E., McCaffrey, K.J.W., Hand, M. (Eds.), Flow Processes in Faults and Shear Zones: Geological Society of London, Special Publication, 224, pp. 1–24.

Durham, W.B., Goetze, C., 1977. Plastic flow of oriented single crystals of olivine. Journal of Geophysical Research 82, 5737–5753.

Frese, K., Trommsdorff, V., Kunze, K., 2003. Olivine [100] normal to foliation: lattice preferred orientation in prograde garnet peridotite formed at high H_2O activity, Cim di Gagnone (Central Alps). Contributions to Mineralogy and Petrology 145, 75–86.

Fuchs, Y., Linares, J., Mellini, M., 1998. Mossbauer and infrared of lizardite-1T from Monte Fico, Elba. Physics and Chemistry of Minerals 26, 111–115.

Ghosh, S.K., Ramberg, H., 1976. Reorientation of inclusions by combination of pure shear and simple shear. Tectonophysics 34, 1–70.

Hanson, D.R., Spetzler, H.A., 1994. Transient creep in natural and synthetic, iron-bearing olivine single crystals: mechanical results and dislocation microstructures. Tectonophysics 235, 293–315.

Heilbronner, R., Tullis, J., 2002. The effect of static annealing on microstructures and crystallographic preferred orientation of quartzites experimentally deformed in axial compression and shear. In: de Meer, S., Drury, M.R., de Bresser, J.H.P., Pennock, G.M. (Eds.), Deformation Mechanisms, Rheology and Tectonics: Current Status and Future Perspectives: Geological Society, London, Special Publications, 200, pp. 191–218.

Hirth, G., Kohlstedt, D.L., 1995. Experimental constraints on the dynamics of the partially molten upper mantle 2. Deformation in the dislocation creep regime. Journal of Geophysical Research 100, 15441–15449.
Hirth, G., Kohlstedt, D.L., 2003. Rheology of the upper mantle and the mantle wedge: a view from the experimentalists. In: Eiler, J. (Ed.), Inside the Subduction Factory. Geophysical Monograph, 136. American Geophysical Union, San Francisco, pp. 83–105.
Holtzman, B.K., Kohlstedt, D.L., Zimmerman, M.E., Heidelbach, F., Hiraga, T., Hustoft, J., 2003. Melt segregation and strain partitioning: implications for seismic anisotropy and mantle flow. Science 301, 1227–1230.
Hoogerduijn Strating, E.H., Rampone, E., Piccardo, G.B., Drury, M.R., Vissers, R.L.M., 1993. Subsolidus emplacement of mantle peridotites during incipient oceanic rifting and opening of the Mesozoic Tethys (Voltri Massif, NW Italy). Journal of Petrology 34, 901–927.
Jin, D., Karato, S.-I., Obata, M., 1998. Mechanisms of shear localization in the continental lithosphere: microstructures of peridotites from the Ivrea zone, northwestern Italy. Journal of Structural Geology 20, 195–209.
Jung, H., Karato, S.-I., 2001a. Water-induced fabric transitions in olivine. Science 293, 1460–1463.
Jung, H., Karato, S., 2001b. Effects of water on dynamically recrystallized grain-size of olivine. Journal of Structural Geology 23, 1337–1344.
Jung, H., Katayama, I., Jiang, Z., Hiraga, T., Karato, S., 2006. Effect of water and stress on the lattice-preferred orientation of olivine. Tectonophysics 421, 1–22.
Jung, H., Mo, W., Green, H.W., 2009. Upper mantle seismic anisotropy resulting from pressure-induced slip transition in olivine. Nature Geoscience 2, 73–77.
Kamb, W.B., 1959. Ice petrofabric observations from Blue Glacier, Washington, in relation to theory and experiment. Journal of Geophysical Research 64, 1891–1909.
Karato, S.-I., Paterson, M.S., FitzGerald, J.D., 1986. Rheology of synthetic olivine aggregates: influence of grain size and water. Journal of Geophysical Research 91, 8151–8176.
Karato, S.-I., Jung, H., Katayama, I., Skemer, P., 2008. Geodynamic significance of seismic anisotropy of the upper mantle: new insights from laboratory studies. Annual Review of Earth and Planetary Sciences 36, 59–95.
Katayama, I., Karato, S.-I., 2006. Effect of temperature on the B- to C-type olivine fabric transition and implication for flow pattern in subduction zones. Physics of the Earth and Planetary Interiors 157, 33–45.
Katayama, I., Jung, H., Karato, S.-I., 2004. New type of olivine fabric from deformation experiments at modest water content and low stress. Geological Society of America Bulletin 32, 1045–1048.
Kelemen, P.B., Dick, H.J.B., 1995. Focused melt flow and localized deformation in the upper mantle: juxtaposition of replacive dunite and ductile shear zones in the Josephine peridotite, SW Oregon. Journal of Geophysical Research 100, 423–438.
Kohlstedt, D.L., Goetze, C., 1974. Low-stress high-temperature creep in olivine single crystals. Journal of Geophysical Research 79, 2045–2051.
Lee, K.-H., Jiang, Z., Karato, S.-I., 2002. A scanning electron microscope study of the effects of dynamic recrystallization on lattice preferred orientation in olivine. Tectonophysics 351, 331–341.
Mackwell, S.J., Kohlstedt, D.L., Paterson, M.S., 1985. The role of water in the deformation of olivine single crystals. Journal of Geophysical Research 90, 11319–11333.
Malahoff, A., 1965. Gravity and geological studies of an ultramafic mass in New Zealand. M.S. Thesis, Hawaii Institute of Geophysics, 20 pp.
Marshak, S., Mitra, G., 1988. Basic Methods of Structural Geology. . 446 pp.
Matsyuk, S.S., Langer, K., 2004. Hydroxyl in olivines from mantle xenoliths in kimberlites of the Siberian platform. Contributions to Mineralogy and Petrology 147, 413–437.
Mei, S., Kohlstedt, D.L., 2000a. Influence of water on plastic deformation of olivine aggregates 1. Diffusion creep regime. Journal of Geophysical Research 105, 21,457–21,469.
Mei, S., Kohlstedt, D.L., 2000b. Influence of water on plastic deformation of olivine aggregates 2. Dislocation creep regime. Tectonophysics 105, 21,471–21,481.
Mercier, J.-C.C., 1985. Olivine and pyroxenes. In: Wenk, H.R. (Ed.), Preferred Orientation in Deformed Metals and Rocks: An Introduction to Modern Texture Analysis. Academic Press, Orlando, Florida, pp. 407–430.
Mercier, J.-C.C., Nicolas, A., 1975. Textures and fabrics of upper-mantle peridotites as illustrated by xenoliths from basalts. Journal of Petrology 16, 454–487.
Michibayashi, K., Mainprice, D., 2004. The role of pre-existing mechanical anisotropy on shear zone development within oceanic mantle lithosphere; an example from the Oman Ophiolite. Journal of Petrology 45, 405–414.
Michibayshi, K., Ina, T., Kanagawa, K., 2006. The effect of dynamic recrystallization on olivine fabric and seismic anisotropy: insight from a ductile shear zone, Oman ophiolite. Earth and Planetary Science Letters 244, 695–708.
Mizukami, T., Wallis, S.R., Yamamoto, J., 2004. Natural examples of olivine lattice preferred orientation patterns with a flow-normal a-axis maximum. Nature 427, 432–436.
Newman, J., Lamb, W.M., Drury, M.R., Vissers, R.L.M., 1999. Deformation processes in a peridotite shear zone: reaction-softening by an H_2O-deficient, continuous net transfer reaction. Tectonophysics 303, 193–222.
Nicolas, A., Poirier, J.P., 1976. Crystalline Plasticity and Solid State Flow in Metamorphic Rocks. John Wiley and Sons, London.
Paterson, M.S., 1982. The determination of hydroxyl by infrared-absorption in quartz, silicate-glasses and similar materials. Bulletin de Mineralogie 105, 20–29.
Raterron, P., Amiguet, E., Chen, J., Li, L., Cordier, P., 2009. Physics of the Earth and Planetary Interiors 172, 74–83.
Sengupta, S., 1997. Contrasting fabrics in deformed dikes and host rocks: natural examples and a simplified model. In: Sengupta, S. (Ed.), Evolution of Geological Structures in Micro- to Macro-scales. Chapman and Hall, London, pp. 341–372.
Skemer, P., Katayama, I., Karato, S.I., 2006. Deformation fabrics of the Cima di Gagnone peridotite massif, Central Alps, Switzerland: evidence of deformation at low temperatures in the presence of water. Contributions to Mineralogy and Petrology 152, 43–51.
Strotzki, W., Wedel, A., Weber, K., Muller, W.F., 1990. Microstructure and texture in lherzolites of the Balmuccia massif and their significance regarding the thermo-mechanical history. Tectonphysics 179, 227–251.
Sundberg, M., Cooper, R.F., 2008. Crystallographic preferred orientation produced by diffusional creep of harzburgite: effects of chemical interactions among phases during plastic flow. Journal of Geophysical Research 113, B12208.
Taylor, W.R., 1998. An experimental test of some geothermometer and geobarometer formulations for upper mantle peridotites with application to the thermobarometry of fertile lherzolite and garnet websterite. Neues Jahrbuch fuer Mineralogie 178, 381–408.
Tikoff, B., Fossen, H., 1993. Simultaneous pure and simple shear: the unifying deformation matrix. Tectonophysics 217, 267–283.
Tikoff, B., Larson, C.E., Newman, J., Little, T., in review. Field-based constraints on finite strain and rheology of the lithospheric mantle, Twin Sisters, Washington. Lithosphere.
Tommasi, A., 1998. Forward modeling of the development of seismic anisotropy in the upper mantle. Earth and Planetary Science Letters 160, 1–13.
Tommasi, A., Mainprice, D., Canova, G., Chastel, Y., 2000. Viscoplastic self-consistent and equilibrium-based modeling of olivine lattice preferred orientations: implications for the upper mantle seismic anisotropy. Journal of Geophysical Research 105 (B4), 7893–7908.
van der Wal, D., Vissers, R.L.M., 1993. Uplift and emplacement of upper mantle rocks in the western Mediterranean. Geology 21, 1119–1122.
Vissers, R.L.M., Drury, M.R., Hoogerduijn Strating, E.H., Spiers, C.J., van der Wal, D., 1995. Mantle shear zones and their effect on the lithosphere strength during continental breakup. Tectonophysics 249, 55–171.
Walcott, R.I., 1965. Structure and petrology of the Red Hill Complex, Nelson. PhD Thesis, Victoria University of Wellington, 274 pp.
Warren, J.M., Hirth, G., 2006. Grain size sensitive deformation mechanisms in naturally deformed peridotites. Earth and Planetary Science Letters 248, 438–450.
Warren, J.M., Hirth, G., Kellermen, P.B., 2008. Evolution of olivine lattice preferred orientation during simple shear in the mantle. Earth and Planetary Science Letters 272, 501–512.
Waters-Tormey, C., Tikoff, B., 2007. Characteristics of a kilometer-scale high strain zone in the lower continental crust: Mt. Hay block, central Australia. Journal of Structural Geology 29, 562–582.
Webber, C.E., 2005. Structural geology of the Porter's Knob area, Red Hills ultramafic massif, New Zealand: Implications for upper mantle deformation. MS thesis. University of Wisconsin-Madison.
Webber, C.E., Little, T., Newman, J., Tikoff, B., 2008. Fabric superposition in upper mantle peridotite, Red Hills, New Zealand. Journal of Structural Geology 30, 1412–1428.
Zhang, S., Karato, S.-I., 1995. Lattice preferred orientation of olivine aggregates deformed in simple shear. Nature 375, 774–777.
Zhang, S., Karato, S.-I., Fitz Gerald, J., Faul, U.H., Zhou, Y., 2000. Simple shear deformation of olivine aggregates. Tectonophysics 316, 133–152.